Buoy perspective of a high-resolution global ocean vector wind analysis constructed from passive radiometers and active scatterometers (1987–present)

Lisan Yu[1] and Xiangze Jin[1]

[1]   The study used 126 buoy time series as a benchmark to evaluate a satellite-based daily, 0.25-degree gridded global ocean surface vector wind analysis developed by the Objectively Analyzed airs-sea Fluxes (OAFlux) project. The OAFlux winds were produced from synthesizing wind speed and direction retrievals from 12 sensors acquired during the satellite era from July 1987 onward. The 12 sensors included scatterometers (QuikSCAT and ASCAT), passive microwave radiometers (AMSRE, SSMI and SSMIS series), and the passive polarimetric microwave radiometer from WindSat. Accuracy and consistency of the OAFlux time series are the key issues examined here. A total of 168,836 daily buoy measurements were assembled from 126 buoys, including both active and archive sites deployed during 1988–2010. With 106 buoys from the tropical array network, the buoy winds are a good reference for wind speeds in low and mid-range. The buoy comparison shows that OAFlux wind speed has a mean difference of -0.13 ms^{-1} and an RMS difference of 0.71 ms^{-1}, and wind direction has a mean difference of -0.55 degree and an RMS difference of 17 degrees. Vector correlation of OAFlux and buoy winds is of 0.9 and higher over almost all the sites. Influence of surface currents on the OAFlux/buoy mean difference pattern is displayed in the tropical Pacific, with higher (lower) OAFlux wind speed in regions where wind and current have the opposite (same) sign. Improved representation of daily wind variability by the OAFlux synthesis is suggested, and a decadal signal in global wind speed is evident.

Citation: Yu, L., and X. Jin (2012), Buoy perspective of a high-resolution global ocean vector wind analysis constructed from passive radiometers and active scatterometers (1987–present), *J. Geophys. Res.*, *117*, C11013, doi:10.1029/2012JC008069.

1.   Introduction

[2] Ocean surface vector wind is a variable of great importance in many oceanic and atmospheric processes, including generating marine waves, driving ocean general circulations, and modulating air-sea fluxes of heat, moisture, and gas fluxes [e.g., *Hayes et al.*, 1989; *Chin et al.*, 1998; *Milliff and Morzel*, 2001; *Josey et al.*, 2002; *Häkkinen and Rhines*, 2004; *Risien and Chelton*, 2008; *Yu*, 2009; *Young et al.*, 2011]. Since the launch of the first Special Sensor Microwave/Imager (SSM/I) on the Defense Meteorological Satellite Program (DMSP) in July 1987, satellite observations of surface winds over the global oceans have been made not only by passive microwave radiometers but also by scatterometers and the recent passive polarimetric microwave radiometer. Scatterometers are microwave radar instruments designed to measure near-surface wind velocity

(both speed and direction) over the oceans [*Naderi et al.*, 1991; *Figa-Saldaña et al.*, 2002]; they surpass passive microwave radiometers [*Hollinger et al.*, 1990; *Wentz*, 1997] that provide only wind speed measurements but no wind direction information. Passive polarimetric microwave radiometer is a new type of passive microwave sensor that is equipped with an ability of retrieving both ocean wind speed and vector through measuring the complex correlation between vertically and horizontally polarized microwave radiation [*Gaiser et al.*, 2004].

[3] Despite the availability of wind data records from more than a dozen satellite wind sensors, characterizing and quantifying the change and variability of global ocean surface wind speed and direction that have occurred during the satellite era is still challenging owing to the lack of a continuous record throughout the entire period. The duration for each sensor varies, lasting from a few months (caused by power failure) to a maximum of 10 years. The SeaWinds scatterometer onboard the National Aeronautics and Space Administration (NASA) QuikSCAT mission between 1999 and 2009 has provided the longest time series of vector wind measurements with research quality [*Risien and Chelton*, 2008; *Vogelzang et al.*, 2011], and has been a vital data source for research and operational applications in a wide range of weather/climate phenomena including tropical

---

[1]Department of Physical Oceanography, Woods Hole Oceanographic Institution, Woods Hole, Massachusetts, USA.

Corresponding author: L. Yu, Department of Physical Oceanography, Woods Hole Oceanographic Institution, MS 21, Woods Hole, MA 02543, USA. (lyu@whoi.edu)
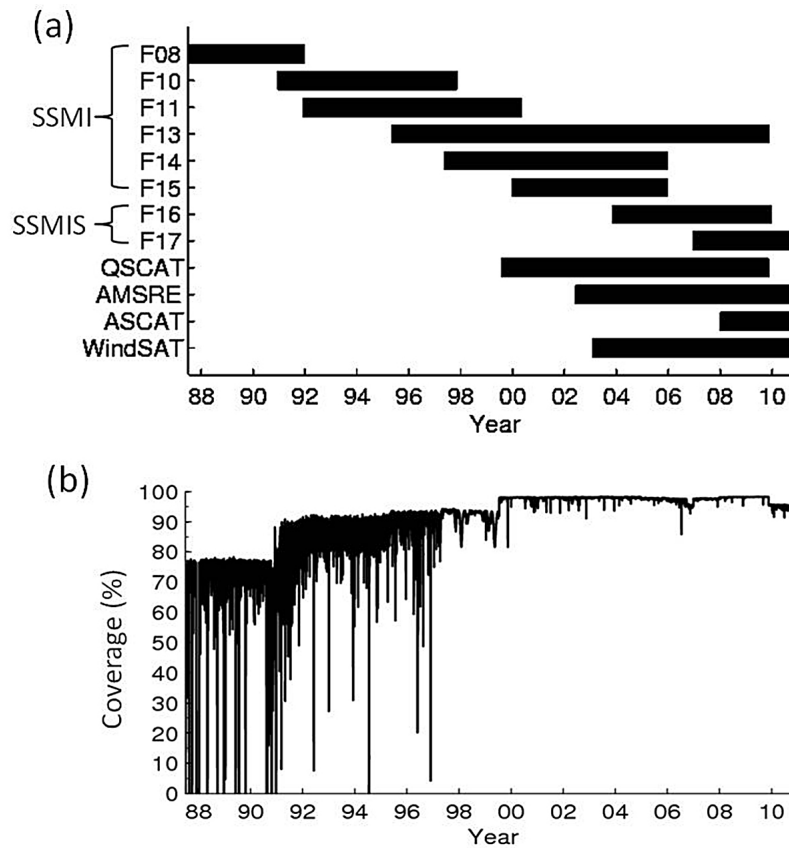
Figure 1. (a) Timeline of the 12 satellite wind sensors included in the OAFlux synthesis. (b) The percentage of the ocean areas covered by the corresponding sensors on a daily basis.

cyclones and El Niño. Presently, two scatterometers have demonstrated significant capability of filling the void left by the loss of QuikSCAT: one is the Advanced scatterometer (ASCAT) system [*Figa-Saldaña et al.*, 2002] that was launched in March 2007 by the European Meteorological Satellite Organization (EUMESAT) operational meteorological satellite system MetOP-A, and the other is the operational satellite OceanSat-2 [*Verhoef and Stoffelen*, 2012a] that was launched in September 2009 by the Indian Space Research Organization (ISRO). If the 10-year QuikSCAT time series can be merged optimally with other scatterometers and passive microwave radiometers to produce a continuous vector wind time series over the entire satellite period, such time series with sufficient accuracy and consistency will undoubtedly bring a greater degree of benefit to the climate/weather studies.

[4] Effort of developing one such time series from synergizing satellite wind observations from multiple sensors and multiple platforms has been made by the Objectively Analyzed air-sea Fluxes (OAFlux) project at the Woods Hole Oceanographic Institution (WHOI). The OAFlux vector wind analysis is an objective synthesis of 12 sensors from 1987 to the present on global 0.25-degree grids and daily resolution. The 12 sensors include two scatterometers, nine passive microwave radiometers, and one passive polarimetric microwave radiometer (Figure 1a and Table 1). The two

Table 1. List of the 12 Sensors, Their Durations, and the Actual Periods Used in the OAFlux Synthesis

Sensor	Duration	Actual Period Being Used
SSMI 08	07/09/87 to 12/31/91	All
SSMI 10	12/08/90 to 11/14/97	All
SSMI 11	12/03/91 to 05/16/00	All
SSMI 13	05/03/95 to 11/18/09	All
SSMI 14	05/08/97 to 08/23/08	05/08/97 to 12/31/05 (Data after 2005 were not used)
SSMI 15	12/18/99 to present	12/18/99 to 6/30/06 (Data after 6/30/06 were not used)
SSMIS 16	10/26/03 to present	10/26/03 to 12/31/09 (Data after 2009 were not used)
SSMIS 17	12/14/06 to present	All
AMSRE	06/01/02 to 11/04/11	All
QuikSCAT	07/19/99 to 11/19/09	All
ASCAT	03/28/07 to present	01/01/09 to present (Data in 2007–08 were not used)
WindSAT	02/05/03 to present	all wind speed retrievals (Direction retrievals were not used)

scatterometers are the QuikSCAT [*Freilich et al.*, 1994] and ASCAT [*Figa-Saldaña et al.*, 2002]. The Indian OceanSat-2 scatterometer measurements were not yet included, as the data set was under evaluation and calibration as to this writing [*Stoffelen and Verhoef*, 2011]. The nine radiometers are the SSMI series on six consecutive DMSP satellites (F08, F10, F11, F13, F14, and F15) [*Hollinger et al.*, 1990], the follow-on Special Sensor Microwave/Imager Sounder (SSMIS) [*Kunkee et al.*, 2008] series onboard DMSP F16 and F17, and the Japanese Advanced Microwave Scanning Radiometer for Earth Observing Systems (AMSR-E) flying aboard the NASA's Aqua satellite [*Kawanishi et al.*, 2003]. The polarimetric microwave radiometer in use is WindSat onboard the U.S. Navy/Air Force Coriolis satellite [*Gaiser et al.*, 2004], which is the first radiometer to measure wind direction. The OAFlux synthesis did not use the European Space Agency's scatterometer carried onboard the Earth Remote Sensing (ERS)-1 and -2 satellites [*Attema*, 1991] because of their narrow swaths and limited spatial coverage on a daily basis. It did not include the short-lived NASA scatterometer (NSCAT) and SeaWinds onboard the Japanese Space Agency's ADEOS-I and -II spacecrafts or the microwave imager onboard the Tropical Rainfall Measuring Mission (TRMM). The latter contains unknown uncertainty incurred by the orbit boost [*DeMoss and Bowman*, 2007].

[5] Constructing satellite-based vector wind time series beyond the 10-year QuikSCAT period has been made by several other groups using various approaches, which include a spline interpolation by *Chin et al.* [1998] and *Milliff et al.* [2004], an optimal interpolation by *Zhang et al.* [2006], *Bentamy et al.* [2007], and *Kako et al.* [2011], and a variational analysis by *Atlas et al.* [2011]. The methodology of the OAFlux vector wind analysis is an advanced statistical approach based on the Gauss–Markov theorem [*Daley*, 1991]. The formulation of a least squares estimator (the so-called cost function) depends on data sets to be synthesized and the problem to be addressed. The best fit to data constraints and the imposed a priori information is sought by a minimization procedure. The same methodology has been applied to produce the OAFlux analysis of global ocean evaporation, latent and sensible heat fluxes [*Yu and Weller*, 2007; *Yu et al.*, 2008]. In principle, all optimal interpolation analyses that are cited above are the best linear unbiased estimator (BLUE). However, the practical approach adopted by each individual in finding the solution to the problem varies considerably. The OAFlux analysis is most similar to the cross-calibrated multiplatform (CCMP) ocean surface wind analysis [*Atlas et al.*, 2011] in that both use a variational minimization to search for an optimal solution. However, the two analyses have two fundamental differences. The first one is the selection of satellite sensors for the synthesis. CCMP includes NSCAT, TMI, and SeaWinds on ADEOS-II while OAFlux does not. On the other hand, OAFlux has four recent sensors, namely, ASCAT, SSMIS F16 and F17, and WindSat to continue the high-resolution vector wind analysis after QuikSCAT, while CCMP does not have these sensors. The second difference is temporal resolution. The CCMP winds are produced on a six-hourly basis by using ECMWF operational analysis to fill in sampling gaps and missing days. By comparison, the OAFlux products are on a daily resolution to maximize the global coverage that satellites can provide. The number of sensors changes throughout the satellite era, with one sensor only at the beginning years (e.g., 1987–1990) and 4–7 sensors at any year after 2000. In the case of one SSMI sensor in operation, about 78% of global oceans cane be sampled in 24 h (Figure 1b) while only about 20% can be covered in six hours when rain-contaminated points are removed. *Vogelzang et al.* [2011] showed in their spectral analysis that ECMWF lacks the small-scale details that are observed by scatterometers. Thus, to ensure good satellite representation at each year over the analysis period, daily resolution appears sensible. Different strategies would lead to different characteristics in the resulting time series. The applicability of OAFlux and CCMP products to weather and climate variability at different time scales, although beyond the scope of this paper, would be a topic worth further investigation. The products from all groups offer an opportunity to cross validate the methodologies in use and to make concerted efforts toward improved documentation and improved characterization of the variability and low-frequency change in global near-surface circulation through maximizing the utilization of all available satellite retrievals.

[6] Wind speed and direction time series acquired from surface moored buoys and research vessels have played a pivotal role in validating satellite wind retrievals [e.g., *Freilich and Dunbar*, 1999; *Mears et al.*, 2001; *Ebuchi et al.*, 2002; *Bourassa et al.*, 2003; *Bentamy et al.*, 2008; *Yu et al.*, 2008; *Vogelzang et al.*, 2011]. Over the satellite period (1987 to the present), we have identified a total of 126 moored surface buoys with research quality that can serve as a validation base to evaluate and quantify the accuracy of the merged OAFlux vector wind time series. Accuracy and consistency are key issues for such time series and will be the focus of investigation here using buoy measurements. The presentation is organized as follows. Section 2 provides a brief description of buoy measurements, satellite wind retrievals, and the winds from the OAFlux analysis. Section 3 presents the buoy evaluation of the OAFlux winds. Outstanding issues are discussed in Section 4. Summary and conclusion is given in Section 5.

2. Data Description

2.1. Buoy Measurements and Accuracy

[7] The location of the 126 buoys is shown in Figure 2 with the OAFlux time-mean field of wind speed and direction superimposed. The latitude/longitude location, the duration, and the total number of available daily measurements for each buoy are listed in Table 2. Among the 126 buoy time series in use, 67 are from the Tropical Atmosphere Ocean/TRIangle Trans-Ocean buoy Network (TAO/TRITON) in the tropical Pacific Ocean [*McPhaden et al.*, 1998], 21 from the Pilot Research Moored Array in the Atlantic (PIRATA) [*Bourlès et al.*, 2008], and 18 from the Research Moored Array for Africa-Asian-Australian Monsoon Analysis and Prediction (RAMA) in the tropical Indian Ocean [*McPhaden et al.*, 2009]. The three tropical array networks constitute a total of 106 buoys. The 20 other buoys include the moored buoys at the Kuroshio Extension Observatory (KEO) [*Cronin et al.*, 2008] and the ocean climate station Papa in the Gulf of Alaska [*Kamphaus et al.*, 2008], and 18 archived/active moored buoys deployed by WHOI at flux reference sites and the sites selected for
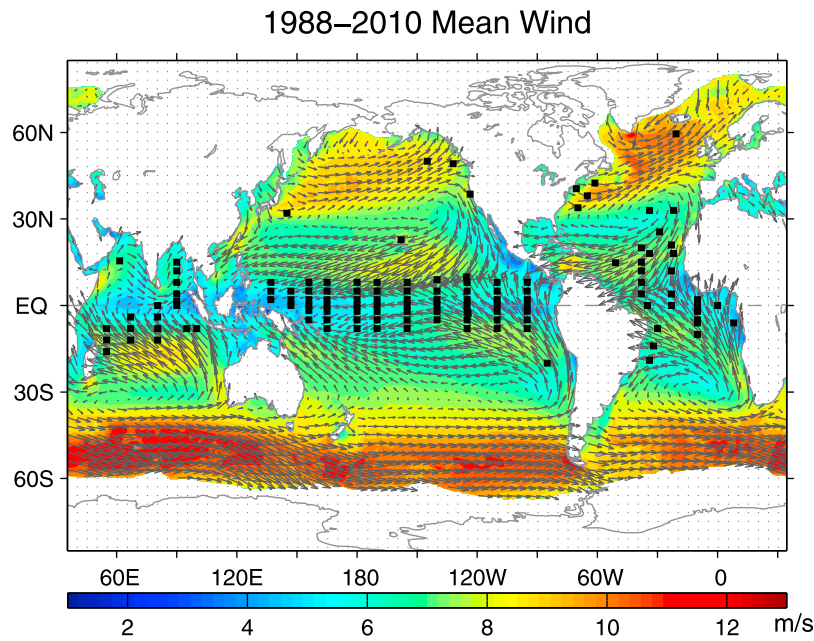
Figure 2. Time-mean wind speed (colored background) and vector produced by the OAFlux global vector wind analysis averaged over the 23 complete years from 1988 to 2010. The superimposed black squares denote the locations of buoys used in the study.

targeted field programs (data are available from http://uop. whoi.edu).

[8] The WHOI buoys are equipped with the Improved METeorology (IMET) or Air Sea Interaction–METeorology (ASIMET) systems [*Weller and Anderson*, 1996; *Moyer and Weller*, 1997]. The three tropical arrays carry the Automated Temperature Line Acquisition System (ATLAS) buoys or TRITON buoys [*McPhaden et al.*, 1998]. A comparison of the ATLAS, TRITON, and IMET mooring meteorological sensors using a land-based cross-validation approach showed that the three systems measure to equivalent standards of accuracy [*Payne et al.*, 2002]. The expected error for the IMET daily averages [*Colbo and Weller*, 2009] is ± 0.1 m s^{-1} (or 1%) in wind speed and $5°$ in wind direction. It is also reported that the error in wind speed measurements under light winds can be larger, at about ± 1 ms^{-1}, because the retarded response of the propeller system makes the buoy unable to orient correctly. The expected error for daily averages from the ATLAS/TRITON instrument [*Freitag et al.*, 2001] is ± 0.3 ms^{-1} (or 3%) for wind speed in the range of 1–20 ms^{-1}, and 5–7.8$°$ in wind direction. Since the ATLAS/TRITON buoys constitute more than 85% of the total buoys in use, the error estimates of these buoys are taken as the standard instrument accuracy in this study.

[9] All satellite winds are calibrated to equivalent neutral winds at 10 m height. Buoy winds are usually sampled at 3–4 m height and transmitted at every 5- or 60-min interval depending upon the design of instruments. For consistency, daily buoy winds (wind speed, direction, zonal and meridional components) were constructed from component averages of the measurements at available sample frequency over each day. Quality control flags in the data files were applied to reject bad or low-quality measurements. These daily buoy winds were then adjusted to the 10 m neutral winds following *Tang and Liu* [1996]. The conversion requires

stability information, such as sea surface temperature (SST), near-surface air temperature and humidity, in addition to wind information, and can be performed only when buoy measurements of all these variables are available. A total of 168,836 daily buoy wind measurements were thus obtained at the 126 buoy locations (Figure 2), and the total number of available daily measurements at each buoy site can be found in Table 2.

2.2. Wind Retrievals and Accuracy

[10] The 12 sensors in the OAFlux synthesis include six SSMIS (F08, F10, F11, F13, F14, and F15), two SSMIS (F16 and F17), AMSRE, WindSat, QuikSCAT, and ASCAT. The time line and duration for each sensor are shown in Figure 1 and Table 1, and a summary of the sensor characteristics and accuracy is given below.

[11] SSM/I is a seven channel passive microwave radiometer operating at four frequencies (19.35, 22.235, 37.0, and 85.5 GHz) and dual-polarization (except at 22.235 GHz which is V-polarization only). SSM/I covers 82% of the earth surface between $87°36′$S and $87°36′$N in 24 h with footprint ranging from 13 km to 69 km, depending on the channel and location along the 1394 km scanning swath [*Hollinger et al.*, 1990; *Wentz*, 1997]. SSMI was first launched onboard the DMSP F8 satellite on 19 June 1987 and subsequent SSMIs have been launched on later DMSP satellites (F10, F11, F13, F14, and F15). Wind speed retrievals are available under both clear and cloud conditions but can be contaminated when cloud/rain liquid water values exceed 18 mg cm^{-2}. *Mears et al.* [2001] showed that mean difference between SSMI winds and buoy winds is less than 0.5 m s^{-1} and the standard deviation of the difference is around 1.3 m s^{-1}.

[12] The SSMIS is the next-generation SSMI. With 24 discrete frequencies from 19 to 183 GHz and a swath

Table 2. List of Buoy Locations, Duration, and Total Number of Days (as of 31 December 2010) Used in the Study[a]

Buoys	Location	Duration	Number of Days (as of 12/31/10)
		The Indian Ocean	
Arabian Sea Experiment	(61.5E, 15.5N)	10/16/94 to 10/19/95	366
RAMA	(55.0E, 16.0S)	10/23/10 to 12/31/10	70
RAMA	(55.0E, 12.0S)	11/23/08 to 12/31/10	165
RAMA	(55.0E, 8.0S)	11/22/08 to 12/31/10	644
RAMA	(67.0E, 12.0S)	09/14/09 to 10/13/09	30
RAMA	(67.0E, 8.0S)	01/14/07 to 10/12/09	942
RAMA	(67.0E, 4.0S)	09/17/09 to 12/24/09	99
RAMA	(80.5E, 12.0S)	05/18/10 to 12/31/10	228
RAMA	(80.5E, 8.0S)	08/23/08 to 11/25/10	809
RAMA	(80.5E, 4.0S)	08/20/08 to 12/31/10	494
RAMA	(80.5E, EQ)	10/23/04 to 03/27/10	564
RAMA	(90.0E, EQ)	09/12/06 to 12/31/10	1041
RAMA	(90.0E, 1.5N)	09/17/06 to 12/31/10	743
RAMA	(90.0E, 4.0N)	11/16/06 to 12/31/10	281
RAMA	(90.0E, 8.0N)	11/14/06 to 12/31/10	755
RAMA	(90.0E, 12.0N)	11/16/07 to 12/31/10	835
RAMA	(90.0E, 15.0N)	11/18/07 to 11/11/10	850
RAMA	(95.0E, 8.0S)	11/14/09 to 04/09/10	147
RAMA	(100.0E, 8.0S)	05/3-/10 to 08/17/10	49
		The Pacific Ocean	
ASREX91	(132.0W, 49.2N)	11/01/91 to 01/06/92	67
COARE	(156.0E, 1.8N)	10/22/92 to 03/03/93	133
KEO	(145.0E, 32.0N)	06/16/04 to 09/05/09	1121
PACS_North	(125.4W, 9.9N)	04/30/97 to 09/13/98	499
PACS_South	(124.6W, 2.8N)	04/21/97 to 09/19/98	514
PAPA	(145.0W, 50.0N)	06/08/07 to 06/07/10	582
SMILE	(123.5W, 38.6N)	11/15/88 to 05/13/89	180
STRATUS	(85.0W, 20.0N)	10/08/00 to 12/31/09	3370
WHOTS	(158.0W, 22.8N)	09/15/04 to 06/05/08	1345
TAO/TRITON	(137.0E, 2.0N)	04/30/93 to 01/21/08	1299
TAO/TRITON	(137.0E, 5.0N)	09/30/01 to 02/01/08	1699
TAO/TRITON	(137.0E, 8.0N)	07/02/02 to 12/31/08	1066
TAO/TRITON	(147.0E, EQ)	04/28/94 to 12/31/08	2970
TAO/TRITON	(147.0E, 2.0N)	05/02/92 to 12/31/08	2421
TAO/TRITON	(147.0E, 5.0N)	12/08/93 to 12/31/08	2901
TAO/TRITON	(156.0E, 5.0S)	09/12/92 to 11/15/08	3040
TAO/TRITON	(156.0E, 2.0S)	07/29/96 to 12/31/08	3312
TAO/TRITON	(156.0E, EQ)	03/02/92 to 12/31/08	3457
TAO/TRITON	(156.0E, 2.0N)	02/22/93 to 09/07/07	3102
TAO/TRITON	(156.0E, 5.0N)	03/04/92 to 12/31/08	3216
TAO/TRITON	(165.0E, 8.0S)	08/29/92 to 02/26/09	2661
TAO/TRITON	(165.0E, 5.0S)	04/20/94 to 02/23/10	3785
TAO/TRITON	(165.0E, 2.0S)	04/18/94 to 11/24/07	2638
TAO/TRITON	(165.0E, EQ)	03/20/91 to 08/16/07	2752
TAO/TRITON	(165.0E, 2.0N)	08/23/92 to 02/17/09	4011
TAO/TRITON	(165.0E, 5.0N)	08/21/92 to 06/15/09	3938
TAO/TRITON	(165.0E, 8.0N)	09/06/90 to 09/05/08	3731
TAO/TRITON	(180.0E, 8.0S)	11/22/93 to 01/12/09	3102
TAO/TRITON	(180.0E, 5.0S)	03/25/93 to 12/31/10	3473
TAO/TRITON	(180.0E, 2.0S)	03/26/93 to 06/27/09	5477
TAO/TRITON	(180.0E, EQ)	03/27/93 to 11/18/06	3628
TAO/TRITON	(180.0E, 2.0N)	03/28/93 to 10/25/10	3869
TAO/TRITON	(180.0E, 5.0N)	06/28/96 to 12/31/10	3406
TAO/TRITON	(180.0E, 8.0N)	12/01/93 to 05/02/09	2786
TAO/TRITON	(170.0W, 8.0S)	08/22/92 to 11/17/09	4222
TAO/TRITON	(170.0W, 5.0S)	11/14/93 to 05/04/09	3297
TAO/TRITON	(170.0W, 2.0S)	11/13/93 to 01/30/10	3048
TAO/TRITON	(170.0W, EQ)	04/16/95 to 08/21/08	3514
TAO/TRITON	(170.0W, 2.0N)	08/24/92 to 02/02/10	3045
TAO/TRITON	(170.0W, 5.0N)	04/05/93 to 08/02/08	3285
TAO/TRITON	(170.0W, 8.0N)	08/26/92 to 03/31/08	4737
TAO/TRITON	(155.0W, 8.0S)	03/06/93 to 09/11/10	5009
TAO/TRITON	(155.0W, 5.0S)	07/23/91 to 01/14/10	4399
TAO/TRITON	(155.0W, 2.0S)	05/24/94 to 09/09/10	3152
TAO/TRITON	(155.0W, EQ)	08/15/92 to 01/11/10	4229
TAO/TRITON	(155.0W, 2.0N)	03/03/93 to 04/15/10	3288
TAO/TRITON	(155.0W, 5.0N)	07/18/91 to 01/09/10	4248
TAO/TRITON	(155.0W, 8.0N)	04/08/95 to 09/04/10	3356
TAO/TRITON	(140.0W, 5.0S)	10/31/90 to 09/04/09	2866
TAO/TRITON	(140.0W, 2.0S)	11/28/91 to 08/30/08	4462

Table 2. (continued)

Buoys	Location	Duration	Number of Days (as of 12/31/10)
TAO/TRITON	(140.0W, EQ)	09/02/09 to 09/02/09	5821
TAO/TRITON	(140.0W, 2.0N)	10/02/98 to 10/28/10	3119
TAO/TRITON	(140.0W, 5.0N)	10/24/90 to 05/16/08	4699
TAO/TRITON	(140.0W, 9.0N)	05/25/94 to 08/29/09	4223
TAO/TRITON	(125.0W, 8.0S)	09/13/96 to 12/31/10	4150
TAO/TRITON	(125.0W, 5.0S)	11/04/91 to 12/31/10	5030
TAO/TRITON	(125.0W, 2.0S)	09/10/94 to 12/31/10	4063
TAO/TRITON	(125.0W, EQ)	09/28/92 to 11/09/08	3458
TAO/TRITON	(125.0W, 2.0N)	05/04/93 to 05/03/09	3699
TAO/TRITON	(125.0W, 5.0N)	12/08/91 to 04/22/10	2429
TAO/TRITON	(125.0W, 8.0N)	09/19/96 to 12/31/10	2255
TAO/TRITON	(110.0W, 8.0S)	03/11/03 to 11/19/05	3111
TAO/TRITON	(110.0W, 5.0S)	03/11/93 to 06/06/06	3292
TAO/TRITON	(110.0W, 2.0S)	05/19/96 to 03/15/10	2082
TAO/TRITON	(110.0W, EQ)	05/09/93 to 02/19/07	2917
TAO/TRITON	(110.0W, 2.0N)	11/04/92 to 07/21/09	2962
TAO/TRITON	(110.0W, 5.0N)	03/15/93 to 11/22/08	3191
TAO/TRITON	(110.0W, 8.0N)	08/24/97 to 08/07/08	2667
TAO/TRITON	(95.0W, 8.0S)	10/19/96 to 09/24/09	3386
TAO/TRITON	(95.0W, 5.0S)	05/13/96 to 12/16/08	2433
TAO/TRITON	(95.0W, 2.0S)	11/15/92 to 07/30/10	1842
TAO/TRITON	(95.0W, EQ)	08/20/95 to 01/02/07	2072
TAO/TRITON	(95.0W, 2.0N)	11/17/92 to 05/27/07	1533
TAO/TRITON	(95.0W, 5.0N)	05/09/96 to 11/05/07	2319
TAO/TRITON	(95.0W, 8.0N)	08/23/95 to 11/18/07	1807
	The Atlantic Ocean		
ASREX93	(69.7W, 33.9N)	12/15/93 to 03/23/94	99
CMO	(70.5W, 40.5N)	07/31/96 to 06/12/97	317
CIMODE	(65.0W, 38.0N)	11/14/05 to 02/08/07	452
MLML91	(20.8W, 59.5N)	04/30/91 to 09/05/91	129
NTAS	(51.0W, 14.8N)	03/31/01 to 02/15/03	687
SESMOOR	(61.2W, 42.5N)	10/18/88 to 03/07/89	141
Subduction	(34.0W, 33.0N)	07/04/91 to 05/31/93	698
Subduction	(34.0W, 18.0N)	06/26/91 to 06/20/93	726
Subduction	(29.0W, 25.5N)	06/24/91 to 06/15/93	723
Subduction	(22.0W, 33.0N)	06/19/91 to 06/13/93	726
Subduction	(22.0W, 18.0N)	06/30/91 to 06/18/93	720
PIRATA	(38.0W, 20.0N)	05/23/07 to 05/13/10	950
PIRATA	(38.0W, 15.0N)	01/29/98 to 07/29/10	2782
PIRATA	(38.0W, 12.0N)	02/04/99 to 06/14/10	2045
PIRATA	(38.0W, 8.0N)	01/31/98 to 01/16/10	2723
PIRATA	(38.0W, 4.0N)	04/12/02 to 01/15/10	2245
PIRATA	(35.0W, EQ)	01/23/98 to 01/17/09	1389
PIRATA	(34.0W, 19.0N)	09/02/05 to 08/29/06	1656
PIRATA	(32.0W, 14.0N)	11/07/06 to 09/01/09	655
PIRATA	(30.0W, 8.0N)	08/22/05 to 12/31/10	1820
PIRATA	(23.0W, EQ)	03/07/99 to 12/31/10	2105
PIRATA	(23.0W, 4.0N)	06/12/06 to 12/31/10	1283
PIRATA	(23.0W, 12.0N)	06/09/06 to 05/17/10	592
PIRATA	(23.0W, 21.0N)	05/20/07 to 05/09/10	736
PIRATA	(10.0W, 10.0S)	09/11/97 to 12/31/10	4011
PIRATA	(10.0W, 6.0S)	03/15/00 to 12/31/10	2551
PIRATA	(10.0W, 5.0S)	01/28/99 to 03/12/00	136
PIRATA	(10.0W, 2.0S)	11/03/99 to 03/03/00	122
PIRATA	(10.0W, EQ)	11/03/99 to 12/31/10	1700
PIRATA	(10.0W, 2.0N)	11/04/99 to 01/05/00	63
PIRATA	(0.0E, EQ)	11/09/98 to 12/31/10	1523
PIRATA	(8.0E, 6.0N)	06/29/06 to 06/08/07	345

[a]There are a total of 126 buoy time series that together provide 168,836 daily wind measurements. Note that actual measurement period at some buoy locations may be longer than listed here. The available time period represents the period that all the four air-sea variables (i.e., wind speed, sea surface temperature, near-surface sir temperature and humidity) are available so that buoy winds can be converted to neutral winds at 10 m.

width of 1700 km, the conically scanning SSMIS offers improved atmospheric temperature soundings, water vapor soundings, and surface observations. SSMIS represents the most complex operational satellite passive microwave imager/sounding sensor ever flown. The instrument became operational in November 2005 onboard the DMSP F16, with one additional onboard F17 in March 2008. Buoy comparisons based on the observations between November 2003 and July 2005 [*Kunkee et al.*, 2008] showed that the performance of SSMIS F16 was very similar to SSMI F13, F14, and F15,

with the mean difference less than 0.2 ms^{-1} for all sensors and a standard deviation between 1.7 and 1.9 ms^{-1}. Here, the shorter study period (21 months) is perhaps the reason that the standard deviations of SSMIs are slighter higher than those mentioned above from *Mears et al.* [2001].

[13] The AMSR-E was launched on 4 May 2002 aboard the NASA's Aqua spacecraft. It is a *dual polarized* microwave radiometer with six frequency channels at 6.9, 10.6, 18.7, 23.8, 36.5 and 89 GHz. The low frequency channels (6.9 and 10.6 GHz) penetrate deeper and are more sensitive to sea surface temperature and wind but less sensitive to the atmosphere [*Meissner and Wentz*, 2002]. The SST and wind speed algorithms are essentially the same, except that the SST algorithm uses all five AMSR-E lower-frequency channels, while the wind algorithm does not use the 6.9 GHz channels because of the lack of improvement. The improved sensitivity of AMSRE to surface wind and temperature improves the accuracy of wind speed retrievals when compared to SSM/I [*Meissner and Wentz*, 2002]. Additionally, AMSR-E scans conically across a 1445-km swath, providing nearly 100% daily coverage for the ocean areas poleward of 45° north and south latitudes and more than 80% daily coverage for the midlatitudes. Comparison of the collocated AMSR-E and TAO buoy winds yielded a mean difference of 0.3 ms^{-1} and the standard deviation of the difference of 1.1 ms^{-1} [*Konda et al.*, 2009].

[14] The WindSat onboard the Air Force Coriolis mission on 6 January 2003 is the first space-based polarimetric microwave radiometer designed to measure the ocean surface wind vector [*Gaiser et al.*, 2004]. The five channels at 6.8, 10.7, 18.7, 23.8 GHz, and 37.0 GHz are similar to those of the AMSR-E sensor except that WindSat does not have an 89 GHz channel. The frequencies at 10.7, 18.7, and 23.8 GHz are fully polarized and these polarization signals contain a small dependence on wind direction that can be used for wind vector retrievals [*Yueh et al.*, 1995; *Laursen and Skou*, 2001]. Studies have shown that WindSat observations are comparable to scatterometers for wind speeds at and above 8 ms^{-1}, but wind direction uncertainty increases substantially for wind speed below 5 ms^{-1} [*Wentz et al.*, 2005; *Quilfen et al.*, 2007]. Daily global coverage of WindSat is approximately 60% of QuikSCAT. Similar to other passive microwave radiometers, there are no WindSat retrievals within about 75 km of the coasts due to contamination by land in the antenna sidelobes. Initial validation results show that wind speed RMS error is less that 2 ms^{-1} for wind speed between 3 and 20 ms^{-1} and wind directional error is less than 25° for wind speeds 5–20 ms^{-1} [*Wentz et al.*, 2005]. Our input data quality control performed before the OAFlux synthesis indicated that WindSat wind direction retrievals have large uncertainties and are not consistent with scatterometer direction retrievals (see also Section 4.1 below for detailed buoy comparison). Thus, OAFlux included only WindSat wind speed retrievals but no direction retrievals.

[15] The SeaWinds on the NASA's QuikSCAT mission is an active radar scatterometer transmitting microwave pulses at a frequency of 13.4 GHz (Ku-band). Wind speed and direction at 10 m above the surface of the water are derived from the backscatter energy. The instrument has an unprecedented large swath width of 1800 km, covering 93% of the global oceans in 24 h, and providing a continuous, high quality ocean vector wind data record for more than 10 years

from 19 June 1999 to 23 November 2009. Accuracy of QuikSCAT wind measurements is estimated at more or less 1 ms^{-1} for wind speed and 20° for wind direction based on concurrent buoy and ship measurements [*Ebuchi et al.*, 2002; *Bourassa et al.*, 2003; *Vogelzang et al.*, 2011]. It is worth noting that the accuracy quoted here cannot be met in the nadir part of the swath, where the QuikSCAT geometry is less favorable for both speed and direction measurement and for rain screening [e.g., *Portabella and Stoffelen*, 2001].

[16] The ASCAT is a C-band (5.255 GHz) dual fan-beam radar scatterometer onboard the EUMETSAT METOP-A satellite on 19 October 2006. MetOp-A will be followed by MetOp-B in 2012 and MetOp-C in 2017, which together will provide for at least 15 years of operational scatterometer data sets. The ASCAT fan-beam antennae cover two 550-km wide swaths separated by a 720 km wide gap, providing about 60–65% of the coverage of QuikSCAT because the latter had a single continuous 1800 km wide swath (no nadir gap). The C-band has a major advantage over the Ku-band in that it is much less affected by direct rain effects, such as ocean splash, and can operate in all-weather conditions. Hence, ASCAT has a unique position of providing reliable observations for the most intense and often cloud-covered wind phenomena, such as polar front disturbances and tropical cyclones. ASCAT and QuikSCAT retrievals agree well for wind speeds in low to moderate range, with the accuracy estimated at 1 ms^{-1} or better for wind speed and 20° for wind direction [*Bentamy et al.*, 2012; *Vogelzang et al.*, 2011]. For higher wind conditions, a few studies [e.g., *Bentamy et al.*, 2008; *Portabella and Stoffelen*, 2009] indicated that effects of increased wind variability appear to dominate ASCAT wind retrievals and cause low wind speed bias.

2.3. The OAFlux Synthesis

[17] The Gauss – Markov theorem is the theoretical background for the OAFlux synthesis [*Daley*, 1991]. It allows the formulation of a least squares estimator (the so-called cost function) to include data from different sources and a priori information that one wishes to impose to constrain the solution. The approach has been used to produce the OAFlux analysis of global ocean evaporation, latent and sensible heat fluxes [*Yu*, 2007; *Yu and Weller*, 2007; *Yu et al.*, 2008]. In developing the OAFlux ocean surface vector wind analysis, a major technical challenge was how to add the directional information to the SSMI wind speed retrievals for the pre-QuikSCAT years when there were no scatterometer data sets in input data sources (Figure 1). In reference to *Hoffman et al.* [2003] and *Atlas et al.* [2011], our strategy was to use the surface vector wind fields from atmospheric reanalysis as a first guess for zonal (u) and meridional (v) wind components, and adjust u and v iteratively by imposing two types of constraints. One is that (i) the analyzed wind speed $w = sqrt(u^2 + v^2)$ should be as close as possible to satellite wind speed retrievals in a least squares sense, and the other is that (ii) the solution of (u, v) should satisfy a set of kinematic constraints such as vorticity and divergence conservations. The addition of vorticity constraints on wind vectors was first developed by *Hoffman* [1984] to remove the ambiguity of the Seasate-A Satellite Scatterometer (SASS) winds. For the years after 1999 when QuikSCAT and later ASCAT became available, scatterometer-based data constraints are included. For the year before 1999 when satellite-based wind direction data are

not available, the neutrally adjusted winds at 10 m from ECMWF-Reanalysis (ERA) interim [*Dee et al.*, 2011] were used as initial conditions.

[18] The OAFlux synthesis obtained the 25 km Level 2 ASCAT wind vectors from the Physical Oceanography Distributed Active Archive center at the Jet Propulsion Laboratory (http://podaac.jpl.nasa.gov/), with the source data at both 12.5 km and 25 km sampling resolution [*Verspeek et al.*, 2010] located at the Ocean and Sea Ice Satellite Application Facility web pages (OSI SAF) at the Royal Netherlands Meteorological Institute (KNMI) (www.knmi.nl/scatterometer) [*Verhoef and Stoffelen*, 2012b]. The data sets of other sensors at 25-km resolution were downloaded from the Remote Sensing Systems company (http://www.ssmi.com/). In particular, the SSMI products were from version 6, SSMIS from version 7, AMSRE from version 5, and QuikSCAT from version 4. The analysis delivers global daily vector wind field on 0.25-degree grids. Daily resolution is selected to ensure maximum satellite coverage over the global oceans at each year throughout the analysis period (Figure 1b).

[19] Rain affects all wind retrievals from all microwave sensors, although rain contamination in the C-band ASCAT is much weaker than in the Ku-band QuikSCAT [*Tournadre and Quilfen*, 2003]. Rain induces a positive bias at low wind speeds due to signal backscatter by raindrops, and a negative bias at high wind speeds due to the atmospheric attenuation of signal. Rain contaminated wind speed and direction data in all sensors were discarded before the OAFlux synthesis by using rain flags contained in the products. Removal of rain contamination reduces the total number of wind retrievals by 5–10%. On a daily basis, all the input sensors in combination cover about 98% of the global oceans during the QuikSCAT period (1999–2009), about 95% for the post-QuikSCAT period (2009-present), and about 78–92% for the pre-QuikSCAT period (1987–1999) (Figure 1b). It appears that there is a need to fill in gaps of missing data if a complete daily global field is desired.

[20] It is a common practice to make the best use of wind fields from numerical weather prediction models to assist the processing of satellite wind retrievals in case of missing/insufficient data. For instance, the removal of directional ambiguity in scatterometer measurements was initialized by the operational 10-m NCEP nowcast analysis to produce the standard QuikSCAT wind products [e.g., *Chelton and Freilich*, 2005]. The six-hourly CCMP wind product [*Atlas et al.*, 2011] applied the 40-year ECMWF Re-Analysis (ERA40) and operational analysis to fill in sampling gaps and to provide the first guess. The model winds used by the OAFlux analysis are the 6-hourly ERA-interim wind (from 1979 onward) with 0.7-degree spatial resolution [*Dee et al.*, 2011]. The data sets were downloaded from the NCAR Research Data Archive at http://dss.ucar.edu. Both the six-hourly downloads and daily mean ERA-interim winds were involved in the daily synthesis. Daily ERA-interim winds (wind speed, direction, zonal and meridional components) were constructed from scalar averaging of the available six-hourly outputs, and they provided the initialization for the OAFlux synthesis. The six-hourly ERA-interim served as the background information to fill in the sampling gaps in input data fields. In other words, the gaps in satellite fields were not filled by daily mean ERA-interim winds but by the nearest six-hourly model winds.

[21] Figure 3 displays the OAFlux analyzed global fields of surface wind speed (w), zonal wind (u), and meridional wind (v) components for the annual mean and the months of January and July averages over the 23 complete years from 1988 to 2010. The mean global wind pattern is clearly shown, with trade winds dominating the tropical oceans and westerlies dominating the midlatitudes between 30 and 60° north and south. The mean pattern is in good agreement with literature [e.g., *Josey et al.*, 2002; *Bourassa et al.*, 2005; *Risien and Chelton*, 2008; *Atlas et al.*, 2011].

2.4. What to Expect From the Buoy Evaluation?

[22] The OAFlux analysis does not synthesize buoy time series. The 126 buoy time series are held as an independent database for two purposes. One is the quality control of input satellite data sets to ensure the quality of the synthesis. Satellite retrievals can drift due to sensor degradation, orbital drift, atmospheric contamination, etc. When the input data are identified with a drift, they are truncated. This is the reason for cutting off SSMI F14 after December 2005, SSMI F15 after June 2006, and SSMIS F16 after December 2009, and excluding ASCAT before January 2009 due to a low bias in wind speed (see Table 1). As suggested by *Vogelzang et al.* [2011], ASCAT was not corrected for equivalent neutral wind before January 2009. This correction is a constant of 0.2 ms^{-1} to the wind speed and only affects the bias of the ASCAT winds but not their error standard deviation. The other use of buoy measurements is the post validation of the synthesized wind fields to ensure the quality of the product.

[23] As shown in Figure 2, existing observations are limited in terms of the geographic coverage. The 126 buoys are all located north of 20°S, with 106 buoys from the three tropical array networks (i.e., RAMA, TAO/TRITON, and PIRATA) between 20°S and 20°N. Therefore, the buoy measurements are most representative of the trade wind regime, where the prevailing northeasterly and southeasterly winds have magnitudes usually not exceeding 15 ms^{-1}. Two wind rose diagrams are displayed in Figures 4a and 4b to depict the percentage of daily wind distribution for the chosen six wind speed categories using the buoy measurements and collocated OAFlux winds at the 126 buoy sites. There are a total of 168,836 daily values in each plot, which represents the total available number of daily buoy measurements across all buoy locations during 1988 and 2010. The two rose diagrams show that the winds over the buoy sites are dominated by easterly trade winds, and that compared to buoys, OAFlux has more wind speeds in the range of 0–8 ms^{-1} and less wind speeds in the range of 8 ms^{-1} and higher.

3. Statistics of OAFlux Wind Speed, Wind Direction, and Wind Components

3.1. Definition of Statistical Measures

[24] The buoy evaluation is based on three commonly used measures. The first one is the overall mean of daily differences between the OAFlux and buoy winds. This measure represents the mean bias of the OAFlux wind time series with regard to buoy measurements. The second measure is the root-mean square (RMS) difference between daily
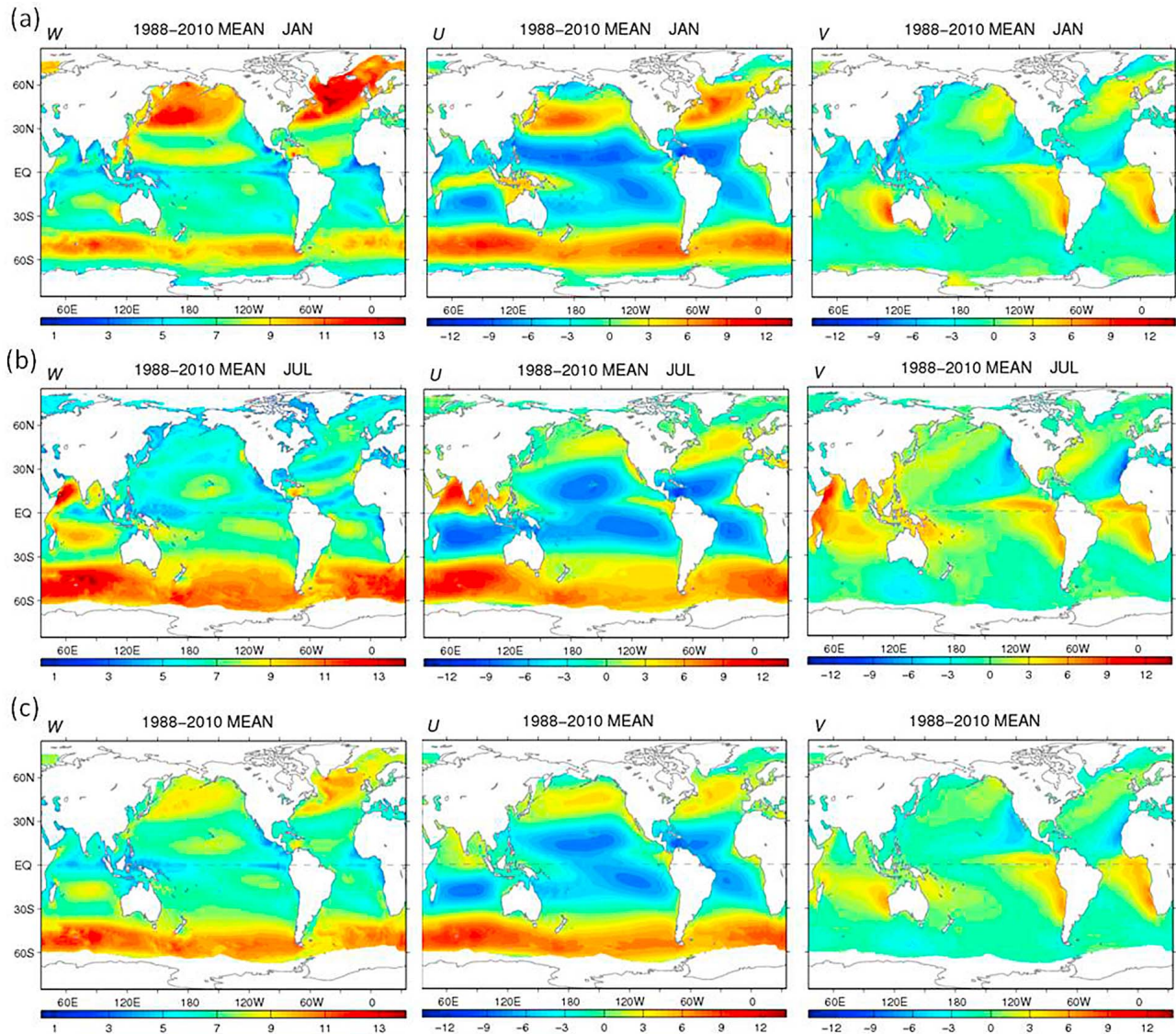
Figure 3. OAFlux mean global fields of near-surface wind speed (w, left), zonal wind component (U, middle), and meridional component (V, right) averaged over the 23 complete years from 1988 to 2010 for (a) January, (b) July, and (c) annual mean.
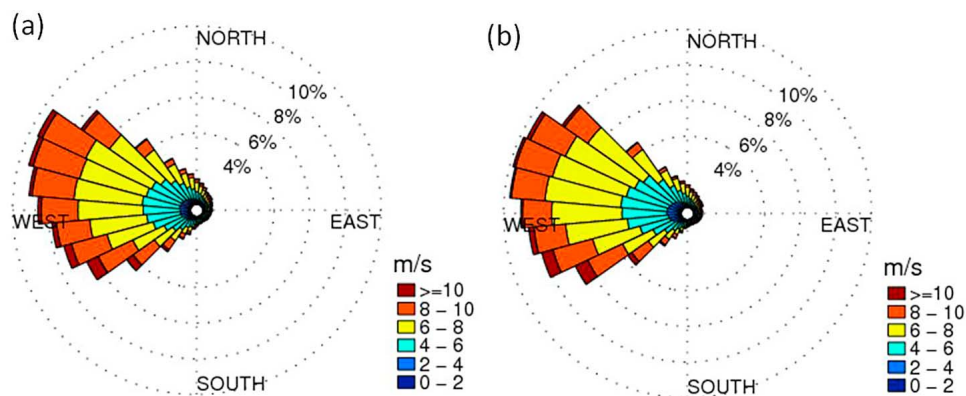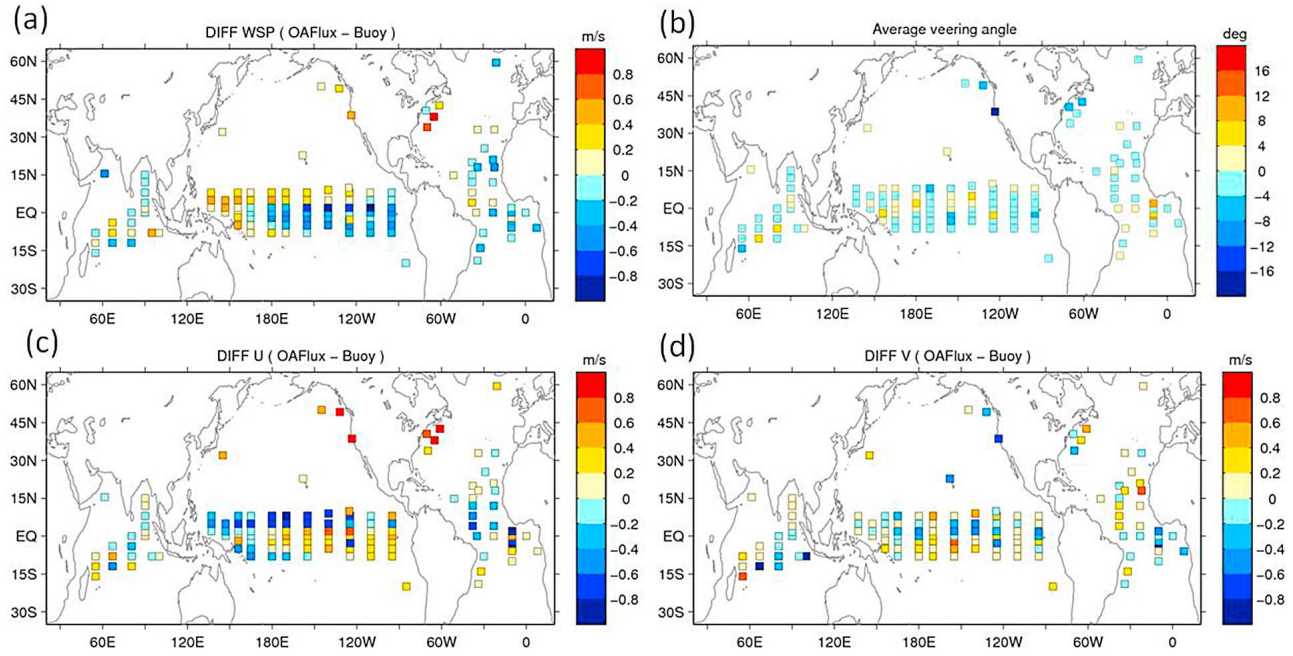

Figure 4. Rose diagram of the percentage of daily wind distribution at all buoy sites from (a) a total of 168,836 buoy daily measurements, and (b) the collocated OAFlux wind analysis. OAFlux has more wind speeds in the range of 0–8 ms^{-1} and less wind speeds in the range of 8 ms^{-1} and higher.

Figure 5. Mean difference between collocated OAFlux and buoy at each buoy site. (a) Wind speed, (b) wind direction, (c) zonal wind component, and (d) meridional wind component.

OAFlux and buoy winds. It is defined as RMS = $\sqrt{\frac{1}{N}\sum_{i=1}^{N}(\chi_i - \chi_{bi})^2}$, where N denotes the total number of daily winds (including speed, direction, zonal, and meridional components) over the 126 buoy locations, x_i is the OAFlux daily wind, and x_{bi} the buoy counterpart. While RMS difference is often applied in buoy comparison studies [e.g., *Ebuchi et al.*, 2002; *Wentz et al.*, 2005; *Quilfen et al.*, 2007], some studies also prefer the use of standard deviation (STD) difference [e.g., *Mears et al.*, 2001; *Bourassa et al.*, 2003; *Kunkee et al.*, 2008]. Although both measures reflect the spread or variability of the analyzed winds relative to buoy measurements, the STD difference is the RMS difference with respect to the mean difference. The third measure is the correlation coefficient (CC) that examines the strength of the linear relationship between daily OAFlux and buoy time series. CC is a scalar measure and computes for each component. For the wind vector time series, a vector correlation would be a better representation of vector (wind speed and direction) differences [*Kundu*, 1976; *Freilich*, 1997; *Bourassa et al.*, 2003]. Following *Kundu* [1976], let $W(t) = u(t) + iv(t)$ be the complex representation of the wind vector at time t, the complex correlation coefficient between vector wind time series of OAFlux (denoted by the subscript "o") and buoy (denoted by the subscript "b") is defined as

$$\rho = \frac{\langle u_b u_o + v_b v_o\rangle}{\langle u_b^2 + v_b^2\rangle^{\frac{1}{2}}\langle u_o^2 + v_o^2\rangle^{\frac{1}{2}}} + i\frac{\langle u_b v_o - u_o v_b\rangle}{\langle u_b^2 + v_b^2\rangle^{\frac{1}{2}}\langle u_o^2 + v_o^2\rangle^{\frac{1}{2}}} \quad (1)$$

The magnitude of ρ gives the overall measure of correlation and the phase angle (i.e., the direction bias of OAFlux relative to buoy), which is written as

$$\alpha = \tan^{-1}\frac{\langle u_b v_o - v_b u_o\rangle}{\langle u_b u_o + v_b v_o\rangle} \quad (2)$$

gives the average counterclockwise angle of the OAFlux vector with respect to the buoy vector. So, if the direction bias is positive, the OAFlux wind veers counterclockwise from the buoy wind.

3.2. Mean Differences: The Influence of Ocean Surface Currents on OAFlux/Buoy Comparisons

[25] Figure 5 shows the mean difference between OAFlux and buoy wind speed (w), wind direction, zonal component (u), and meridional component (v) at the 126 buoy locations. Data record length differs with location, ranging from a few months to more than a decade (Table 2). Nevertheless, the OAFlux-buoy difference is within ± 0.4 ms^{-1} in w, and within ± 4 degrees in wind direction over most buoy sites. Magnitude of the mean difference in w is due more to u and less to v. Strikingly, the mean difference pattern in w shows an organized structure in the tropical Pacific: a band of negative differences (weaker OAFlux w) in the eastern and central equatorial Pacific surrounded by bands of positive differences (stronger OAFlux w) to the north and west. This pattern mirrors that of the mean difference in u albeit with opposite signs. Wind component is a vector and can be both negative and positive, unlike wind speed which is a scalar and always positive. Given that the winds are predominantly westward in the tropical Pacific (Figure 2), a positive bias in u indicates a weaker u and weaker w and conversely, a negative bias in u indicates a stronger u and stronger w.

[26] *Kelly et al.* [2001] pointed out that satellite wind retrievals represent the winds relative to the moving ocean surface, not the winds relative to a stationary point such as the anemometer measurements from buoys. The satellite-derived wind speed should be lower than the anemometer wind speed when the current is in the same direction as the wind, and higher when the current is in the opposite direction as the wind [see *Kelly et al.*, 2001, Figure 1]. The effect
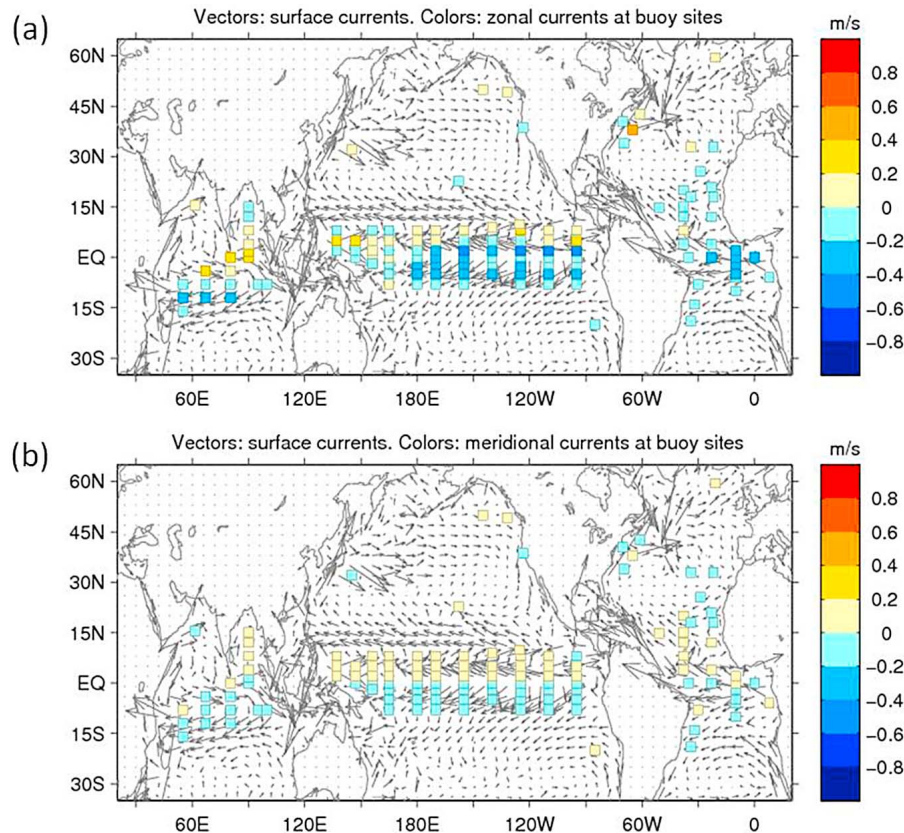
Figure 6. (a) Mean zonal near-surface currents at the buoy sites (colors) superimposed onto mean surface current vectors (background gray arrows). Positive (negative) denote eastward (westward) flows. (b) Same as Figure 6a but for mean meridional near-surface currents. Positive (negative) values denote northward (southward). The mean surface currents (vectors) are obtained from a drifter-derived climatology.

of ocean surface currents on the mean difference pattern in w and u can be elucidated using Figures 6a and 6b, which is the vector map of a drifter-derived climatology of near-surface currents [*Lumpkin and Garraffo*, 2005] superimposed with zonal and meridional currents at buoy sites. In the equatorial Pacific, the eastward-flowing North Equatorial Countercurrent (NECC) dominate the buoy sites between 2°N and 10°N and the westward-flowing South Equatorial Current (SEC) dominate the buoy sites south of 2°N. OAFlux w is stronger than buoy w (positive bias) when the local current is eastward and opposite to the prevailing trade wind, whereas OAFlux w is weaker than buoy w (negative bias) when the local current is westward and in the same direction as the prevailing trade wind. Zonal currents from *Lumpkin and Garraffo* [2005] have a magnitude generally less than 0.3 ms^{-1}, which appears to be comparable to the magnitude of the mean differences in w at most buoy locations. Meridional currents are usually weaker ($<0.1 \text{ ms}^{-1}$) and the effect is not readily discernible. Similar current effect, albeit weaker, is also seen in the tropical Atlantic.

[27] One question arises. If ocean currents are the major contributor to the discrepancies between OAFlux and buoy winds as suggested by Figures 5 and 6, should the differences between the two winds agree with the magnitude of ocean surface currents? *Kelly et al.* [2005] hypothesized that the differences in buoy/scatterometer measurements should be the ocean surface currents and attempted the inference of

the time-varying ocean surface currents from differences between QuikSCAT and TAO winds. One major obstacle in addressing this question is the lack of direct surface current measurements. *Kelly et al.* [2005] made use of near-surface current estimates from all available sources including currents at 15-m depth from drifters, at 25-m depth from acoustic Doppler current profilers (ADCPs), and at 10-m depth from current meters. It should be noted that surface currents are different from near-surface currents at 10-m and below, due to the vertical shear in the geostrophic currents and to the Ekman currents. In light of the sparse direct near-current observations and large uncertainties in each instrument, here we rely on the near-surface current climatology derived from drifter measurements at 15-m depth [*Lumpkin and Garraffo*, 2005] (Figures 6a and 6b) to produce a first-order quantification of the ocean current effect. The climatological near-surface currents are not the "truth" and do not represent the surface condition, but they are generated from the same platform and should have consistent error characteristics across the area of study.

[28] Figure 7 shows the mean comparison of zonal components in the equatorial Pacific, as the correlation for the meridional wind differences and meridional currents is weak. For the convenience of comparison, the direction of the zonal OAFlux-buoy differences is reversed in the plot so that the vectors represent the zonal buoy-minus-OAFlux differences, which is different from other figures that are all
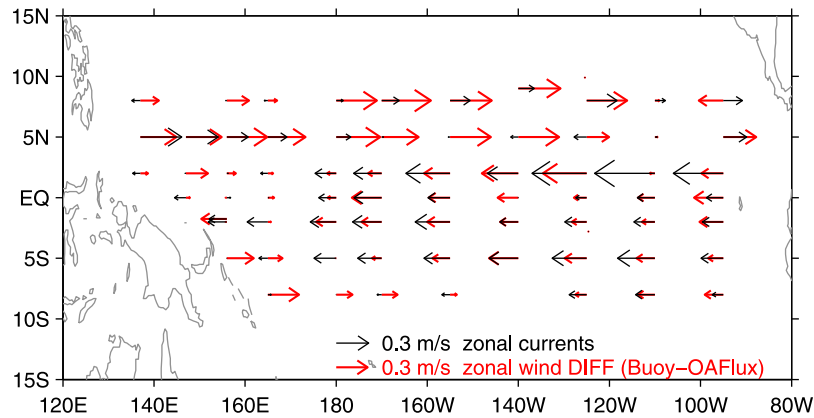
Figure 7. Evaluation of the effect of zonal currents (black vectors) in the equatorial Pacific on Buoy-OAFlux differences for zonal wind component (red vectors). Note that the zonal wind difference vectors denote the buoy-minus-OAFlux which is opposite to all other figures.

based on the OAFlux-minus-buoy differences. By doing so, the magnitude of the ocean current climatology can be directly compared to the magnitude of the mean buoy/satellite differences. Evidently, zonal mean wind differences are in good agreement with the zonal current climatology: both are westward in the SEC-dominated eastern and central equatorial Pacific where the winds blow with the surface currents and OAFlux winds are weaker, and both are eastward in the NECC regions north of the equator (5–10°N) where the winds blow against the surface currents and OAFlux winds are stronger. Estimates of the SEC explain well the mean zonal wind differences in the region, although the currents are slightly stronger than the differences of the two zonal winds. Current divergence about the equator is observed, which is suggestive of an Ekman response [*Kelly et al.*, 2005], and the zonal wind

differences have a similar divergence feature. It is interesting that the satellite-based OAFlux winds could be reasonable zonal current meters in the SEC region.

[29] On the other hand, estimates of the NECC are not sufficient to account for the large differences in the two wind systems, although the two are mostly in the same direction. The OAFlux can be 0.4–0.6 ms^{-1} stronger than the buoy winds while the currents estimates seldom exceed 0.3 ms^{-1}. It is not yet clear what caused the large discrepancies between zonal currents and the mean zonal wind differences between buoy and OAFlux.

3.3. RMS Differences and Vector Correlations

[30] Figure 8 shows the RMS differences between daily OAFlux and buoy w, direction, u, and v. The RMS error for
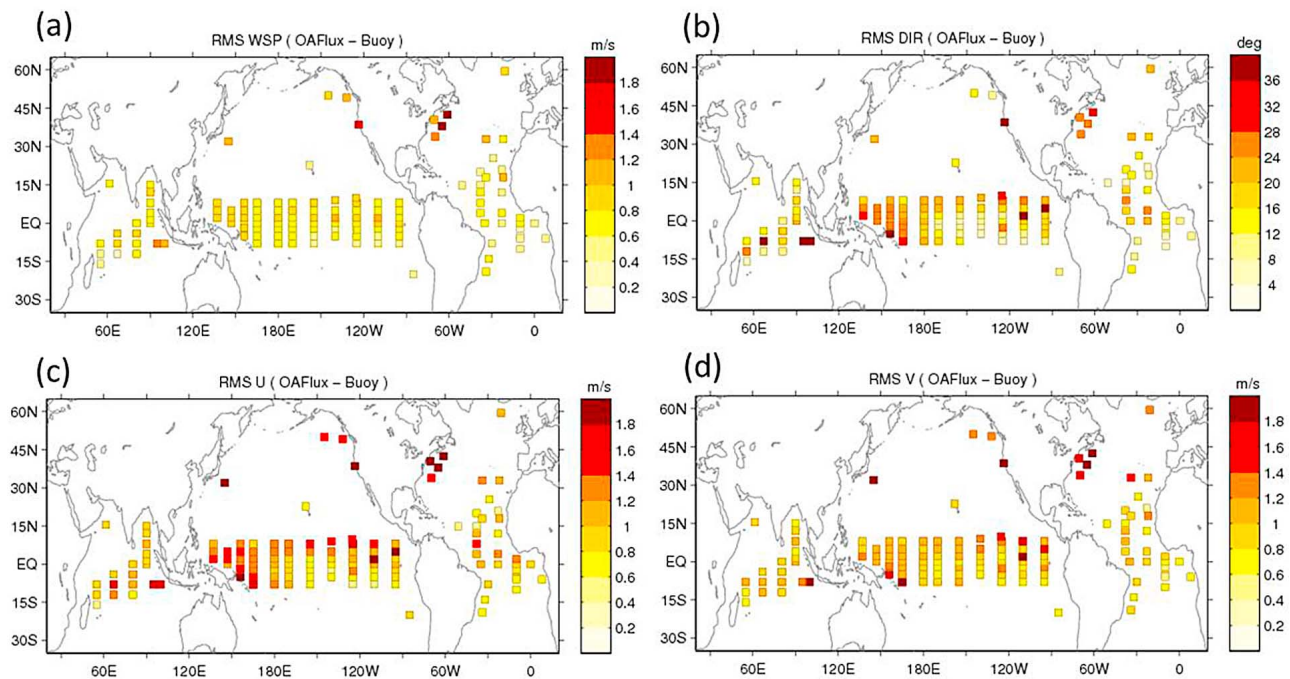

Figure 8. RMS of daily difference between OAFlux and buoy at each buoy site. (a) Wind speed, (b) wind direction, (c) zonal wind component, and (d) meridional wind component.
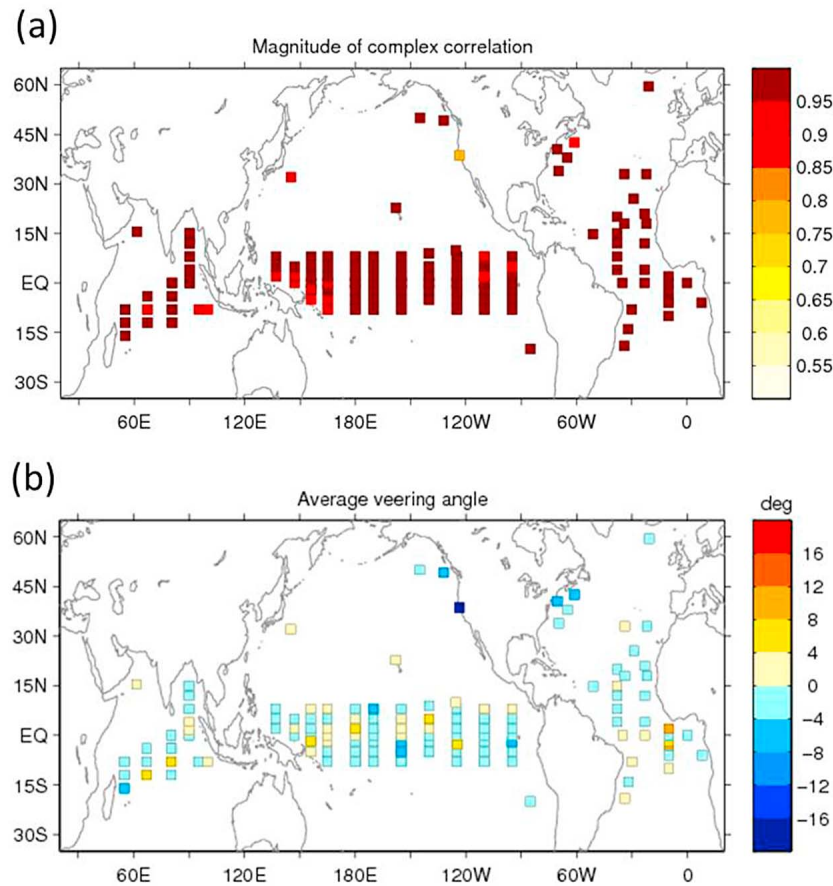
Figure 9. (a) Vector correlation coefficients between daily OAFlux and buoy vector winds at all buoy sites, and (b) the corresponding wind direction bias (i.e., difference between OAFlux and buoy in wind direction).

the OAFlux w ranges between 0.2–0.8 ms^{-1} at most tropical buoy locations, but is greater than 1.2 ms^{-1} at the four buoys sites in the vicinity of the Gulf Stream where winds are usually strong (>10 ms^{-1}). The effect of zonal currents is visible in the RMS error pattern for u, producing larger RMS in regions of the NECC where currents and winds have opposite directions, and weaker RMS in regions of the SEC where currents and winds are in the same direction. Daily vector wind variability between OAFlux and buoy computed from equations (1) and (2) shows high correlation coefficients (Figure 9). The magnitude of the complex correlation is 0.9 and higher across all buoy sites, except for one site 38°40′N, 123°30′W on the Northern California shelf. This site was placed for the Shelf Mixed Layer Experiment (SMILE) that was designed to study the response of the oceanic surface boundary layer over the continental shelf to atmospheric forcing during November 1988 – May 1989 [*Alessi et al.*, 1991]. Among all sites, the correlation at this site is lowest (0.84) and the direction bias is largest (−16°). Positive direction biases denote that the OAFlux winds veer counterclockwise from the buoy winds, while negative direction biases denote that the OAFlux winds veer clockwise from the buoy winds. Microwave passive radiometers have limited availability within 75 km away from the coast due to contamination from the antenna sidelobes. The

SMILE buoy is about 70 km from the coast, which might be a reason for the observed low correlation coefficient.

3.4. Scatterplots

[31] Comparison of OAFlux daily winds with collocated buoy daily winds is summarized in the scatterplots (Figure 10) and Table 3. There are a total of 168,836 buoy/OAFlux collocations across the 126 sites. Using the buoy measurements as a reference, the OAFlux w has a mean difference of −0.13 ms^{-1} and an RMS difference of 0.71 ms^{-1}, while the wind direction has a mean difference of −0.56 degrees and an RMS difference of 17.34 degrees. Given that the instrument accuracy of the buoys is ±0.3 ms^{-1} for wind speed and ±5–7.8 degrees for wind direction, the mean differences of OAFlux wind speed and vector is within instrument accuracy.

[32] The scatterplot for wind direction shows that larger spreads are observed when the directions are near 0°/360° and wind components are weak. The scatters plots of OAFlux u and v versus buoy u and v show a poorer fit for the wind components within the range of ±5 ms^{-1}, but a good linear fit for wind components beyond ±5 ms^{-1}. At weak winds, technical problems exist in both buoy measurements and satellite retrievals. The propeller system on buoys has a retarded response to very low winds, causing error in wind speed as large as ±1 ms^{-1} [*Colbo and Weller*, 2009].
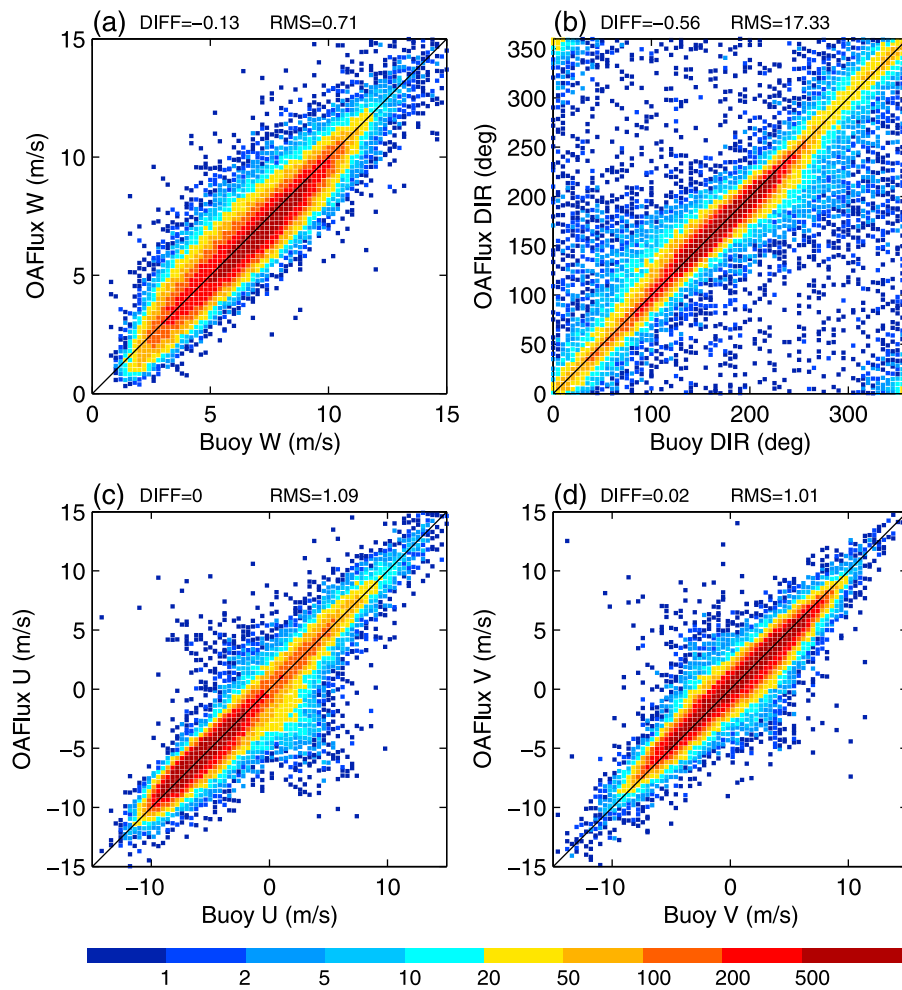
Figure 10. Scatterplots of collocated OAFlux and buoy measurements for (a) wind speed, (b) wind direction, (c) zonal wind component, and (d) meridional wind component. There are a total of 168,836 collocations for the period between 1988 and 2010.

Scatterometer retrievals also have difficulty to determine wind direction in light wind conditions and require a direction selection from multiple possible solutions (known as ambiguity). The ambiguity removal is over 99% effective for wind speed of 8 ms^{-1} – 20 ms^{-1} but degrades considerably for weak winds due to low signal/noise ratio [*Naderi et al.*, 1991; *Gonzales and Long*, 1999; *Bourassa et al.*, 2003]. The overall comparison with buoy shows that OAFlux u has an RMS difference of 1.09 ms^{-1} and a mean difference of 0.00 ms^{-1}, while OAFlux v has an RMS difference of 1.01 ms^{-1} and a mean difference of 0.02 ms^{-1}. The correlations

of the OAFlux w, direction, u, v with the buoy counterparts are high, at 0.94 and higher (Table 3), all significant at 95% confidence level.

[33] To evaluate the impact of including scatterometers on the synthesis and the representation of the statistics of the entire time series, we divided the 23-year period into two parts, the pre-1999 period from 1988 to 1998 and the post-1999 period from 2000 to 2010, and computed the buoy-based statistics for each period and added to Table 3. It should be noted that the total number of collocations summing over the two periods is not equal to the total collocation

Table 3. Statistics of Buoy Evaluation of OAFlux Wind Speed, Direction, and Zonal and Meridional Wind Components for Three Periods 1988–2010, 1988–1998, and 2000–2010[a]

	1988–2010 N = 168,836			1988–1998 N = 10,093			2000–2010 N = 152,239		
	DIFF (ms^{-1})	RMS (ms^{-1})	cc (0–1)	DIFF (deg)	RMS (deg)	cc (0–1)	DIFF (ms^{-1})	RMS (ms^{-1})	cc (0–1)
w (ms^{-1})	−0.13	0.71	0.94	−0.22	0.86	0.93	−0.13	0.66	0.95
DIR (degree)	−0.55	17.34	0.95	2.47	19.8	0.96	−0.90	16.98	0.95
u (ms^{-1})	0.00	1.09	0.96	0.01	1.18	0.96	−0.01	1.03	0.96
v (ms^{-1})	0.02	1.01	0.96	−0.15	1.22	0.96	0.05	0.98	0.96

[a]Note that the sum of the number of collocations (N) of the latter two periods is less than the total number of the entire period because the year 1999 is not included. Three statistical properties are listed, including mean difference (DIFF), root-mean square (RMS) error, and correlation coefficient (cc).
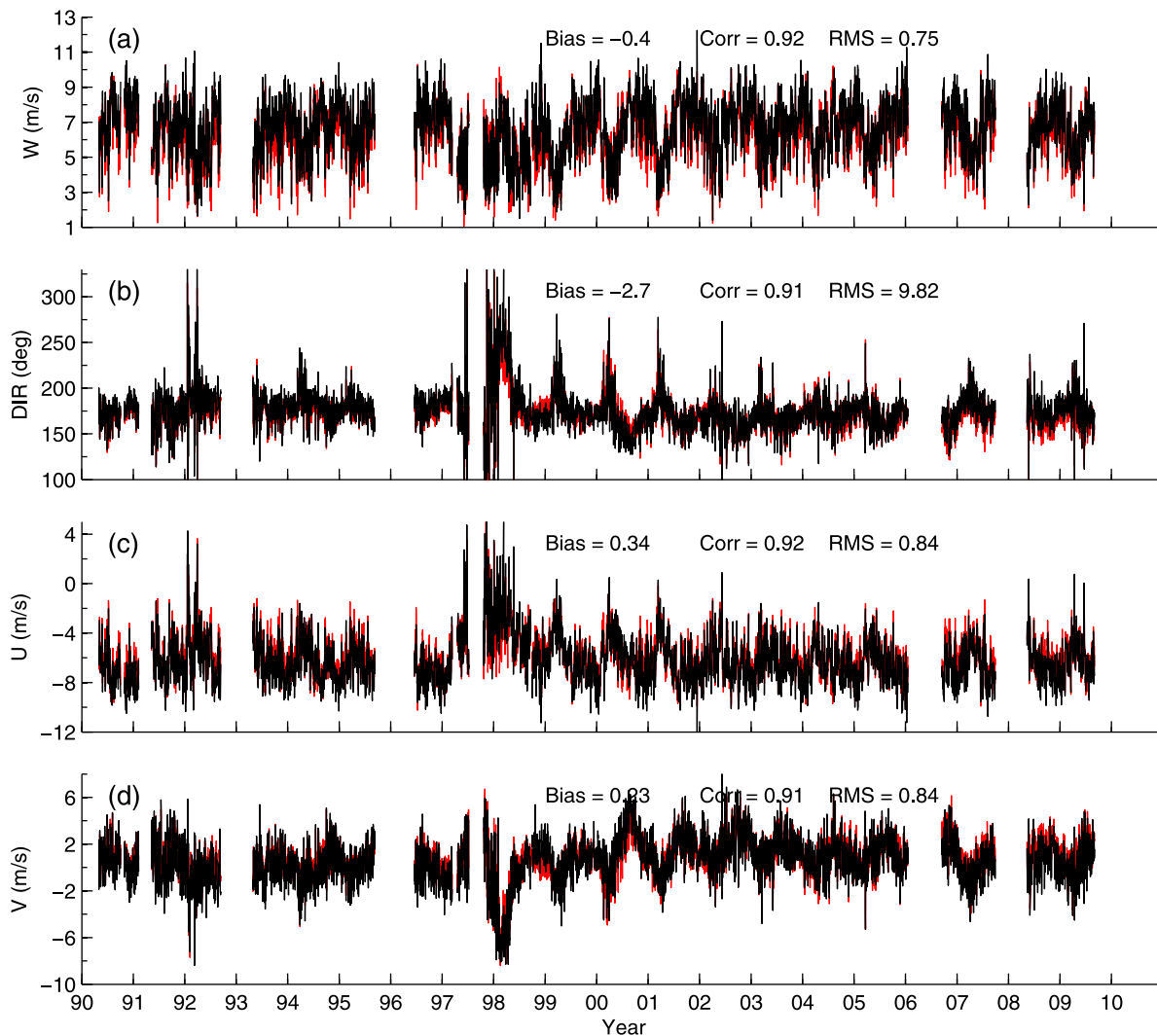
Figure 11. Time series of daily buoy winds (black) versus OAFlux winds (red) at the TAO/TRITON buoy location 140W, 0N. (a) Wind speed, (b) wind direction, (c) zonal wind component, and (d) meridional wind component.

number (168,863) over the entire period from 1988 to 2010, because the year 1999 is not included in either period. It should also be kept in mind that available buoy samplings for the pre-1999 period are at most one-tenth of that for the post-1999 period. Error statistics is influenced by the sampling size: the larger the sampling size, the more accurate the error statistics. A slight degradation in mean and RMS differences for the pre-1999 period is expected when comparing with the post-1999 period. Except for CC that shows not much change between the two periods with coefficients all above 0.9 for all components, the mean and RMS differences show a slight increase for the pre-1999 period.

3.5. Time Series at TAO and PIRATA Buoy Sites

[34] Several TAO buoys were deployed in the early 1990s (see Table 2) during the early stage of the international Tropical Ocean Global Atmosphere (TOGA) program [*McPhaden et al.*, 1998]. These buoy time series of ~20 years encompasses much of the analysis period from July 1987 to present, providing a valuable reference for validating the

consistency of the OAFlux analysis before, during, and after QuikSCAT (1999–2009). One of such buoys, 140°W, 0°N, has a start date in 1990 and is taken to evaluate the OAFlux daily winds at the location (Figure 11). Correlation coefficients at 0.91 and higher are shown for all OAFlux/buoy pairs (w, dir, u, and v). The mean OAFlux w is about 0.4 ms^{-1} weaker than the mean buoy w, because the wind at this location blows with local currents (Figures 5–7), thus weaker zonal winds (positive bias) and weaker wind speed (positive bias) are resulted. The RMS daily differences between the two winds are 0.75 ms^{-1}, 0.84 ms^{-1}, and 0.84 ms^{-1} for w, u, and v, respectively. However, the surface drifter climatology [*Lumpkin and Garraffo*, 2005] shows the zonal current at this equatorial location is -0.013 ms^{-1}, which is far from sufficient to justify that ocean currents are the cause of the large discrepancies between the two zonal winds of 0.34 ms^{-1}. The lack of agreement between climatological current estimates and the 20-year zonal mean differences in OAFlux/Buoy underlines the crucial role of data accuracy in assessing the ocean current effect on the satellite/buoy comparison studies.
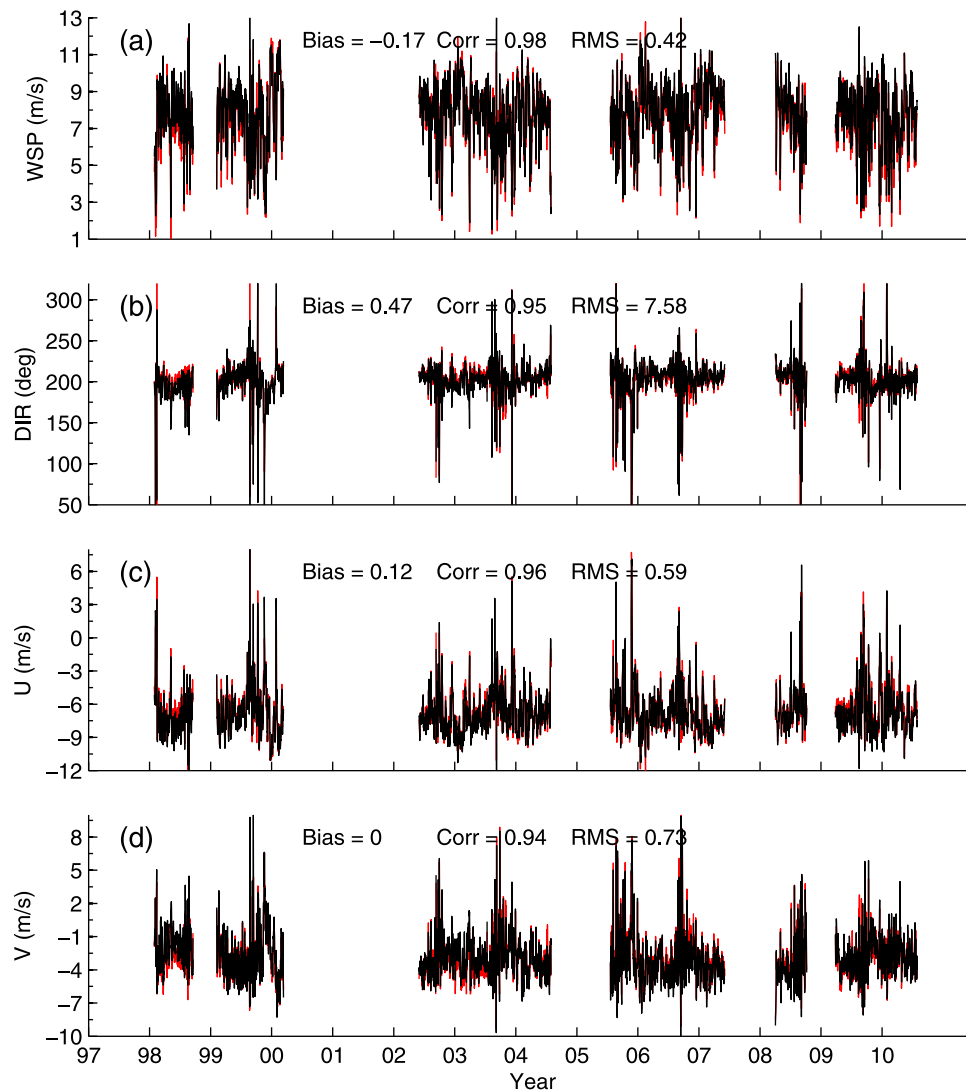
Figure 12. Time series of daily buoy winds (black) versus OAFlux winds (red) at the PIRATA buoy location 38W, 15N. (a) Wind speed, (b) wind direction, (c) zonal wind component, and (d) meridional wind component.

At this location, daily buoy wind STD variability is 1.60 ms^{-1} and the STD OAFlux/buoy difference is 0.62 ms^{-1}. The ratio between the two STDs is 0.38, implying that the OAFlux/buoy STD difference accounts for 38% of the buoy STD daily variability.

[35] Another time series comparison is shown in Figure 12 based on a PIRATA buoy at 38°W, 15°N. The PIRATA program started in late 1997 with the full array in place by 2000 [*Bourlès et al.*, 2008]. The chosen buoy has time series dating back to early 1998, but the time series is fragmentary with missing measurements in some years. Similar to the comparison at the TAO buoy site, daily variability of the OAFlux winds agrees well with that of the buoy winds. The CCs for wind speed, direction, u and v components are all 0.94 and higher. The RMS daily differences between OAFlux and the buoy is 0.42 ms^{-1}, 0.59 ms^{-1}, and 0.73 ms^{-1} for w, u, and v, respectively, and is 7.6 degrees for wind direction. Mean differences are low for all components, with -0.17 ms^{-1}, 0.12 ms^{-1}, and 0.0 ms^{-1} for w, u, and v, respectively, and 0.47 degrees for wind direction. The daily

PIRATA buoy wind STD variability is 1.70 ms^{-1} and the STD OAFlux/buoy difference is 0.38 ms^{-1}. Hence, the OAFlux/buoy STD difference is about 22% of the buoy STD daily variability.

[36] A good consistency between OAFlux and the buoy is observed throughout the entire analysis period. The same conclusion can also be drawn for the comparisons at other buoy sites as well. It appears that the OAFlux framework of synergizing ASCAT, SSMIS and WindSat is able to compensate the loss of QuikSCAT after 2009.

4. Discussion

4.1. OAFlux Versus Input Satellite Sensors

[37] Theoretically, the objective synthesis of multiple sensors should lead to a vector wind field with improved accuracy, because the combined use of multiple sensors provides better global coverage and more samples to use in constructing a daily mean field. Each sensor provides at most two samples per day at each grid location. The number
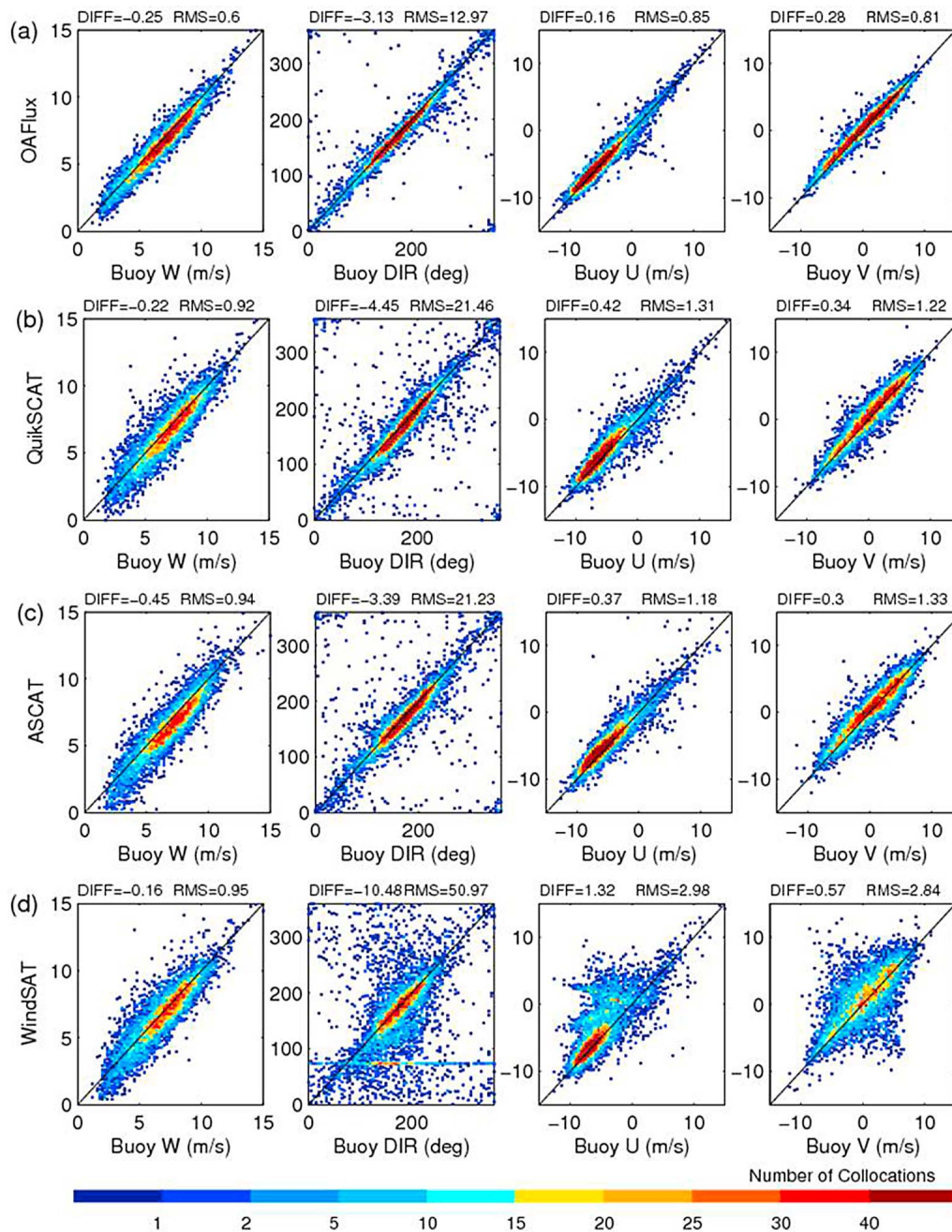
Figure 13. Scatterplots for (a) OAFlux-buoy, (b) QuikSCAT-buoy, (c) ASCAT-buoy, and (d) WindSat-buoy for wind speed (first column), wind direction (second column), zonal wind (third column), and meridional wind (fourth column). The plots are based on a total of 7660 collocations between the seven participating sensors (four in this figure and three in the next) and buoy measurements during 2008–09.

of sensors included in OAFlux ranges from two to seven except for the first three years (Figure 1), which gives 2–14 samples for computing daily mean. Theoretically, the synthesis process tends to cancel out errors in input data sets and produces an estimate that has the minimum variance [*Daley*, 1991]. Hence, the synthesis represents an improved representation over input data sets. To elucidate this point, here we evaluate the accuracy of input satellite winds against OAFlux winds using collocated buoy measurements (Figures 13 and 14). The overlapping two-year period from 1 January 2008 to 31 December 2009 was selected from a constellation of seven sensors, including SSMI F13, SSMIS F16 and F17, AMSRE, WindSat, QuikSCAT, and ASCAT. These seven sensors together with buoys yielded 7660 collocations for the two years. Figure 13 shows the collocated vector wind analysis for OAFlux/buoy, QuikSCAT/buoy, ASCAT/buoy, and WindSat/buoy, while Figure 14 shows the collocated wind speed comparisons for SSMI F13/buoy, SSMIS F16/buoy, SSMIS F17/buoy, and AMSRE/buoy. The statistics (e.g., mean difference, rms, and CC) of the buoy evaluation are summarized in Table 4.
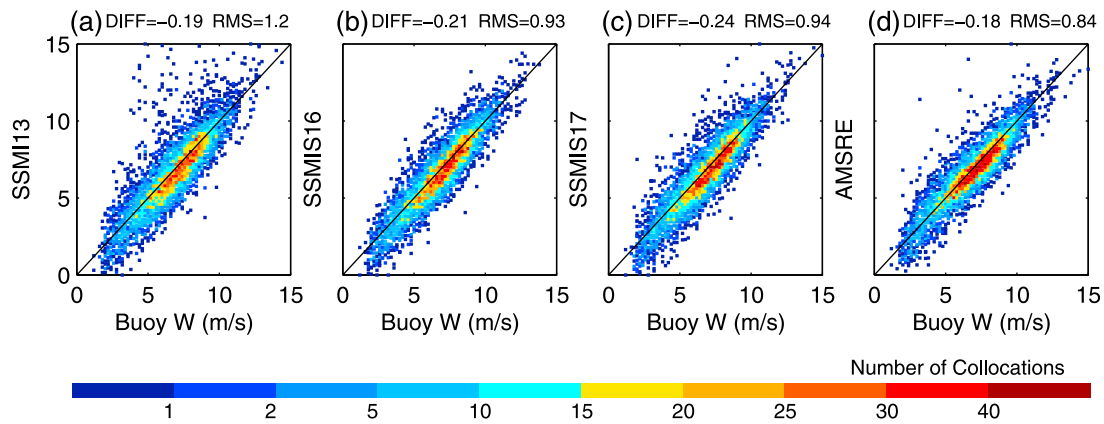
Figure 14. Scatterplots of wind speed for (a) SSMI F13-buoy, (b) SSMIS F16-buoy, (c) SSMIS F17 – buoy, and (d) AMSRE-buoy based on a total of 7660 collocations between the seven participating sensors (three in this figure and four in the next) and buoy measurements during 2008–09.

[38] Compared to the seven sensors, OAFlux winds have the best agreement with buoy winds. The OAFlux/buoy pairs cluster more closely around the straight line (i.e., the ideal fit) than all other pairs, with the CCs for w, u, and v all above 0.96. OAFlux has the lowest RMS differences and the highest CC for all four quantities (w, dir, u, and v) (Table 4). Mean difference between OAFlux and buoy w is -0.25 ms^{-1}, well within the instrument accuracy of ± 0.3 ms^{-1}. Among the seven sensors, the statistics of w from the four radiometers (SSMI, SSMIs, and AMSRE) is comparable to the scatterometer retrievals (QuikSCAT and ASCAT). WindSat w is in good agreement with buoy w, but there is a significant RMS difference (rms > 50 degree and CC < 0.4) in wind direction. It has been reported that the accuracy of the WindSat wind direction retrievals strongly depends on wind speed [*Yueh and Wilson*, 1999; *Meissner and Wentz*, 2002; *Wentz et al.*, 2005]. WindSat direction is comparable to that of QuikSCAT for wind speed greater than 7 ms^{-1}, but the accuracy degrades rapidly for wind speed less than 5 ms^{-1}. It is likely that the poor comparison in wind direction in Figure 13 is due to large errors in WindSat wind direction of low winds. The large uncertainty in WindSat wind direction is the reason that only WindSat wind speed was included in the synthesis.

[39] Since OAFlux represents an ensemble mean in a sense, one would expect that the errors in OAFlux should drop by ∼1/(sqrt(N)) compared to input sensors, where N is the number of sensors used. As is shown in Table 4, the reduction in errors made by OAFlux is not as steep as the theoretical projection. One main reason is that the errors in sensors are correlated and the covariances between N sensors are not zero (for instance, the correlation of errors between QuikSCAT and SSMI16 is 0.35). The considerable correlations between sensors impose a limit to the degree of error reduction that can be achieved by a synthesis. Nevertheless, the OAFlux synthesized daily wind products have an improved statistics of daily winds judged from either the total buoy comparison with 168,836 collocations or the two-year comparison with 7660 collocations.

4.2. OAFlux Versus ERA-Interim

[40] ERA-interim winds are an auxiliary data set in the OAFlux synthesis to supply the background information when data are missing and to provide the first guess for wind direction during the least squares fitting. ERA-interim is a practical simulation of the state of the atmosphere using a state-of-the-art assimilation system. Surface winds assimilated by ERA-interim include not only satellite passive microwave radiometers (SSMI, SSMIS, and AMSRE) and scatterometers (ERS-1, ERS-2, and QuikSCAT) but also in situ wind measurements from buoys and ships [*Dee et al.*, 2011]. OAFlux does not include in situ observations, but overlaps with ERA-interim in satellite data sources. OAFlux

Table 4. Statistics of Buoy Evaluation of OAFlux and Seven Input Sensors for the 2008–09 Period[a]

	w			DIR			u			v		
	DIFF (ms^{-1})	RMS (ms^{-1})	cc (0–1)	DIFF (deg)	RMS (deg)	cc (0–1)	DIFF (ms^{-1})	RMS (ms^{-1})	cc (0–1)	DIFF (ms^{-1})	RMS (ms^{-1})	cc (0–1)
OAFlux	-0.25	**0.60**	**0.96**	-3.13	**12.97**	**0.88**	**0.16**	**0.85**	**0.97**	**0.28**	**0.81**	**0.98**
QuikSCAT	-0.22	0.92	0.90	-4.45	21.46	0.77	0.42	1.31	0.93	0.34	1.22	0.95
ASCAT	-0.45	0.94	0.92	-3.39	21.23	0.74	0.37	1.18	0.94	0.30	1.33	0.94
WindSat	**-0.16**	0.95	0.89	-10.48	50.97	0.39	1.32	2.98	0.74	0.57	2.84	0.72
SSMI F13	-0.19	1.20	0.85	-	-	-	-	-	-	-	-	-
SSMIS F16	-0.21	0.93	0.91	-	-	-	-	-	-	-	-	-
SSMIS F17	-0.24	0.94	0.91	-	-	-	-	-	-	-	-	-

[a]There are a total of 7660 collocations for the constellation of seven sensors and buoys. Three statistical properties are listed, including mean difference (DIFF), root-mean square (RMS) error, and correlation coefficient (cc). Minimal mean difference and RMS values and maximal correlation coefficient are shown in bold font. For w, instrument accuracy is ± 0.3 ms^{-1}. For DIR, instrument accuracy is ± 5–7.8 degrees.
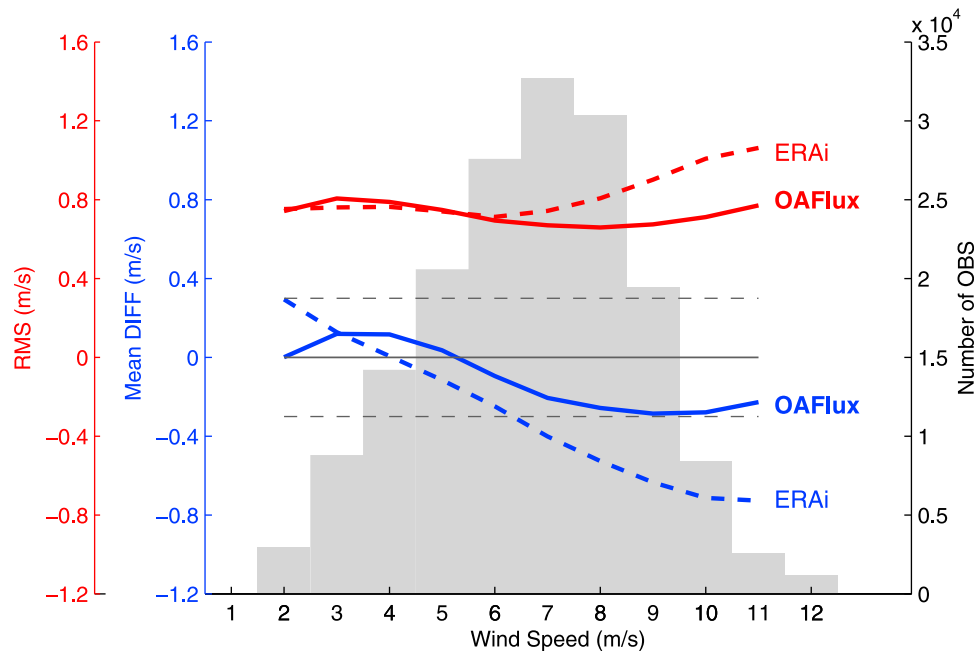
Figure 15. Comparison of mean difference (blue) and RMS difference (red) between daily OAFlux and buoy (solid lines) versus the mean and RMS differences between daily ERAinterim and buoy (dashed lines). The gray dashed line denotes the ± 0.3 ms^{-1} accuracy of buoy wind speed measurements. The background gray bar plot shows the distribution of the number of buoy measurements with wind speed.

and ERA-interim employ different methodologies (i.e., a statistical objective analysis versus an atmospheric general circulation model with data assimilation), but the mean spatial pattern of the near-surface wind circulation from the two systems are in good agreement (not shown). One question is then to what degree the synthesized fields represent an improvement over the ERA-interim reanalysis wind fields.

[41] To address this question, the neutrally adjusted 10 m ERA-interim winds are evaluated using the same 168,836 daily buoy measurements as shown above and compared with OAFlux. Figure 15 shows the comparison of the buoy-based mean and RMS differences of the two winds over the background of the density distribution of buoy wind speed. One notable feature is that the mean and RMS differences between ERA-interim and buoys increase with increasing wind speed. By contrast, the mean difference of OAFlux w is within the buoy measurement accuracy of ± 0.3 ms^{-1} at all wind speed ranges, albeit OAFlux w seems to be slightly higher than buoy at low winds and slightly lower than buoy for winds greater than 6 ms^{-1}. The RMS difference of OAFlux w is around 0.8 ms^{-1} across all buoy wind speeds, while the RMS difference of ERA-interim w is a function of wind speed and reaches up to 1.1 ms^{-1} when w is 11 ms^{-1}. Higher winds (>11 ms^{-1}) were recorded primarily by the buoys in the vicinity of the Gulf Stream (Figure 5) and account for a scant 0.7% of the total buoy measurements. The sampling size is not sufficient to provide a statistically significant evaluation for w greater than 11 ms^{-1}, and hence, winds higher than 11 ms^{-1} are excluded in Figure 15.

[42] It should be noted that ocean currents do not influence the buoy evaluation of ERA-interim winds, because NWP model winds are the winds relative to a stationary point in a way similar to the anemometer measurements from buoys.

Though ERA-interim assimilates surface wind retrievals from scatterometers and microwave radiometers, the reanalysis winds are not satellite winds. There is no signature of ocean currents in the mean difference pattern between ERA-interim and buoy winds (not shown), which is unlike OAFlux (Figures 5 and 7). When averaged over the total buoy measurements, the mean ERA-interim w differs from buoys by -0.34 ms^{-1} which is beyond the buoy instrument accuracy of ± 0.3 ms^{-1}. The weaker ERA-interim w can be interpreted as the actual underestimation bias in ERA-interim winds. This assessment is consistent with existing literature reporting that NWP winds are weak biased compared to buoy and satellite winds [e.g., *Jiang et al.*, 2005; *Wallcraft et al.*, 2009; *Vogelzang et al.*, 2011].

[43] Comparison of OAFlux and ERA-interim in the conditions of tropical storms is shown in Figures 16 and 17. OAFlux does not contain rain-affected wind retrievals. Rain contamination on satellite wind retrievals is most severe in tropical storm events [*Stiles and Yueh*, 2002; *Weissman et al.*, 2002; *Draper and Long*, 2004; *Hilburn et al.*, 2006] and is a major contributor to gaps in input data. To fill in the gaps, the six-hourly ERA-interim winds that are closest to the time of satellite observations were employed as background information to assist the construction of the synoptic structure. Figure 16 displays the surface wind speed and wind convergence fields from OAFlux and ERA-interim winds associated with Hurricane Katrina on 28 August 2005, about one day before it made landfall in Louisiana. The reanalysis winds are the daily average of six-hourly fields. The plots have surface wind streaklines superimposed onto surface wind convergence (i.e., $\partial u/\partial x + \partial v/\partial y$; positive upward). Note that streaklines differ from streamlines in that the former are the locus of points of all the fluid particles that
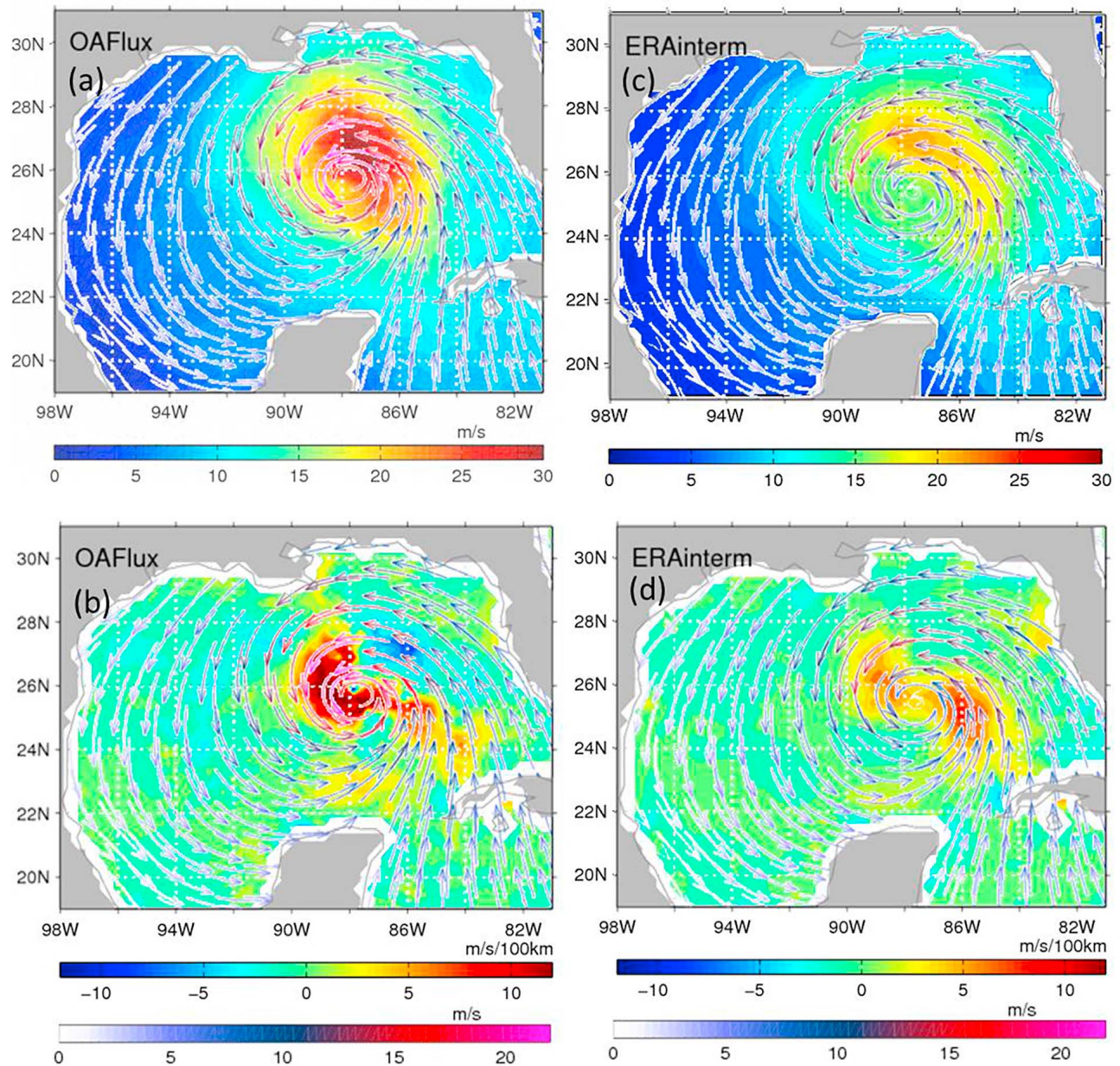
Figure 16. (a) OAFlux daily surface wind speed and (b) wind convergence (positive)/divergence (negative) associated with Hurricane Katrina on 28 August 2005. Surface wind streaklines are superimposed in both plots. (c and d) The same as Figures 16a and 16b but for ERA-interim daily mean that was constructed from averaging six-hourly winds.

have passed continuously through a particular spatial point in the past, while the latter a family of curves that are instantaneously tangent to the velocity vector of the flow.

[44] It can be seen from Figure 16 that the two wind streakline fields produced a similar cyclonic structure, with peak wind speed located in the right-front quadrant of the storm. Nonetheless, details of the synoptic fields differ considerably. OAFlux winds are obviously stronger and have a finer depiction of the surface convergence field. For instance, the storm's eye is seen in OAFlux, but not in the reanalysis. The maximum surface convergence was located in the left-front quadrant in OAFlux where heavy rainfall was reported [*Lau et al.*, 2008], while ERA-interim has the

maximum convergence in the right-rear quadrant. Apparently, the use of the 6-hourly ERA-interim winds as backup information did not turn OAFlux into a model wind.

[45] Figure 17 provides another example of surface wind streakline and convergence fields associated with Hurricane Bonnie on 25 August 1998. Similar to the Hurricane Katrina case discussed above, OAFlux differs from ERA-interim in the magnitude of wind speed, the storm's eye structure, and the location of the maximum surface convergence. Interestingly, the OAFlux synthesis before September 1999 does not include scatterometer sensors and the initialization of the minimization process was provided by ERA-interim. Hence, the improved representation of the storm's surface wind
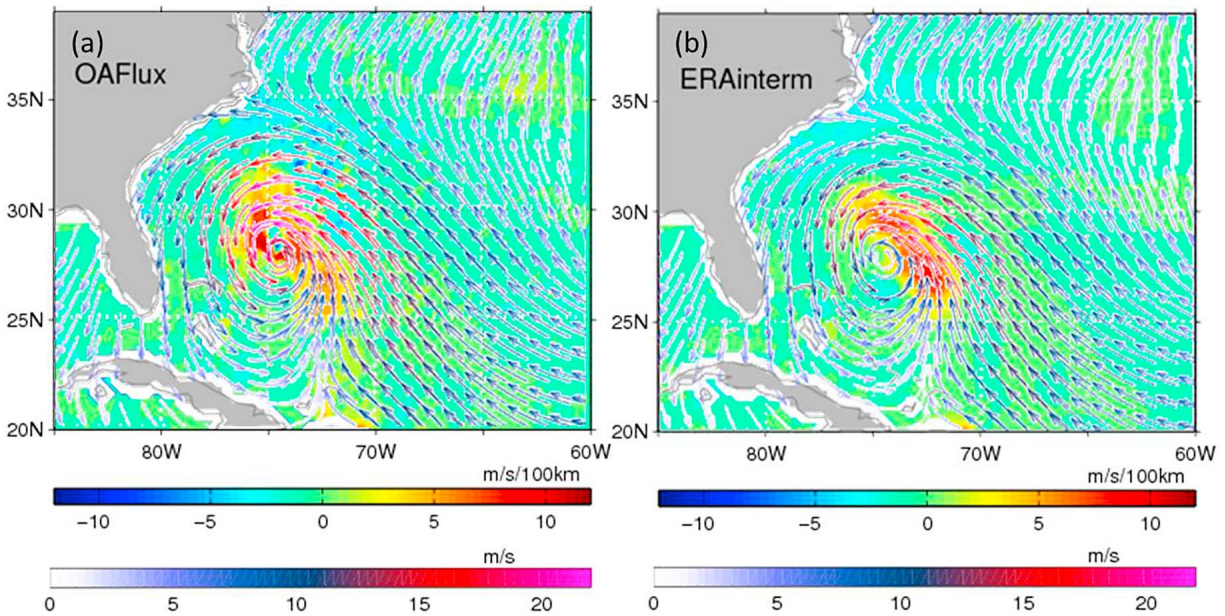
Figure 17. Daily mean surface wind streaklines and wind convergence (positive)/divergence (negative) associated with Hurricane Bonnie on 25 August 1998 using winds from (a) OAFlux and (b) ERA-interim.

structure associated with Hurricane Bonnie is attributed to the synthesis of satellite wind speed observations from passive radiometers. The use of ERA-interim as the first guess helped the synthesis process but the coarse structure of the reanalysis wind field did not influence the synthesized wind fields. The advantage of synthesis is shown.

[46] *Vogelzang et al.* [2011] conducted spectral analysis to wind fields from ASCAT, QuikSCAT, and ECMWF operational forecast and found that the model winds miss small spatial scale details observed by the scatterometers, although they have similar large spatial scale structures. The spectra of the ECMWF winds falls off more rapidly than the scatterometer wind spectra starting at scales of about 1000 km, indicating less variance at high spatial frequencies. This study found that ERA-interim winds misrepresent the fine spatial structures associated with hurricane conditions, and is consistent with the findings of *Vogelzang et al.* [2011]. A spectral analysis is a useful tool for identifying the spatial

representation scale of the wind product [*Milliff and Morzel*, 2001; *Chelton et al.*, 2006]. Such analysis would be a necessary step for a comprehensive characterization of the OAFlux winds merged from 12 satellite sensors; however, the topic is beyond the scope of the present study and will be pursued through ongoing study.

4.3. Yearly Mean Time Series of OAFlux, ERA-Interim, and 12 Input Sensors

[47] The low bias in ERA-interim winds is also evident when comparing the annual-mean time series of globally averaged wind speed with those constructed from OAFlux and from the 12 input sensors used by OAFlux (Figure 18). The reanalysis w is consistently lower than all satellite wind sensors as well as the OAFlux synthesis during the 23 complete years from 1988 to 2010. The mean difference between OAFlux and ERA-interim w is 0.33 ms^{-1} for the 23-year global averages, which is comparable to the mean difference
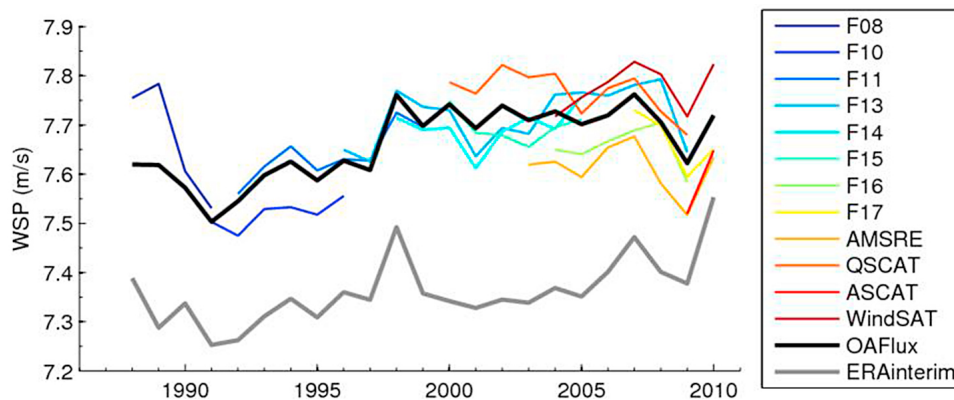

Figure 18. Annual-mean time series of OAFlux, ERAinterim, and the 12 input sensors used in the OAFlux analysis.

between the two wind products at the 126 buoy sites (not shown).

[48] Different sensors have different mean states. For instance, the mean state of QuikSCAT and WindSat w is about 0.05 ms^{-1} higher than SSMI and SSMIS, while the mean state of AMSRE and ASCAT is about 0.06 ms^{-1} lower. The OAFlux mean state was strategically made to follow the mean state of SSMI and SSMIS, because these two types of sensors are best calibrated [*Wentz*, 1997] and provide by far the longest consistent record of global wind speed. However, not all SSMI and SSMIS retrievals are useful. As shown in Table 1, retrievals from SSMI F14 after December 2005, SSMI F15 after June 2006, and SSMIS F16 after December 2009 were excluded due to a drift in the mean. Similarly, ASCAT retrievals before January 2009 were also discarded due to a low bias compared to other sensors. As suggested by *Vogelzang et al.* [2011], ASCAT retrievals were not corrected for equivalent neutral wind before January 2009 and this correction is a constant of 0.2 ms^{-1} to the wind speed.

[49] The annual-mean time series of input sensors shown in Figure 18 is the actual data record included in the synthesis, not the actual duration of each sensor. The OAFlux synthesis stands as an optimal representation of 12 input sensors. It follows the tendency of all input sensors, but has a mean state that agrees more with SSMI sensors. It is observed that OAFlux differs from ERA-interim not only in the mean magnitude of w but also in low-frequency tendency. Distinct decadal variations in OAFlux w are seen, characterized by a rapid intensification in the 1990s and a rather flat tendency during most of the 2000s. A sharp reduction in wind speed occurred in 2008–09. On the other hand, ERA-interim depicts a low-frequency intensification of global averaged wind speed throughout the entire satellite era. It is noted that the ensemble view pieced together by all the satellite sensors does not support the picture produced by ERA-interim. The 10-year QuikSCAT time series shows that the globally averaged ocean vector wind speed has a slight downward trend when taking into account of the dip in 2008–09. WindSat and AMSRE have a similar tendency though the mean state differs by 0.1 ms^{-1}. The SSMIs and SSMISs in combination also suggest a steady low-frequency mode. There is no sign of an increase of global mean wind speed from satellites.

5. Summary and Conclusions

[50] The study used 126 buoy time series as a benchmark to evaluate a satellite-based daily, 0.25-degree gridded global ocean surface vector wind analysis developed by the OAFlux project. The OAFlux winds were produced from synthesizing wind speed and direction retrievals from 12 sensors acquired during the satellite era from July 1987 onward. The 12 sensors included scatterometers (QuikSCAT and ASCAT), passive microwave radiometers (AMSRE, SSMI and SSMIS series), and the passive polarimetric microwave radiometer from WindSat (Figure 1 and Table 1). Accuracy and consistency of the OAFlux time series are the key issues examined in the study. Five major findings are summarized as follows.

[51] 1. A total of 168,836 daily surface wind measurements were assembled from the 126 buoy times series acquired between 1988 and 2010 (Figure 2 and Table 2).

The instrument accuracy of the buoys is ±0.3 ms^{-1} for wind speed and ±5–7.8 degree for wind direction. The study showed that the collocated OAFlux wind speeds have a mean difference of −0.13 ms^{-1} and an RMS difference of 0.71 ms^{-1}, and wind directions have a mean difference of −0.56 degree and an RMS difference of 17 degrees. Vector correlation of collocated OAFlux and buoy winds is of 0.9 and higher over almost all buoy sites. The average direction bias is between −4° and 4°. A summary of the buoy evaluation is included in Figure 10 and Table 3.

[52] 2. Ocean surface currents exert strong influence on OAFlux wind speed in the equatorial Pacific Ocean (Figures 5 and 6). Higher OAFlux wind speeds are found in the region of the North Equatorial Countercurrent where winds blow against currents have the opposite sign, and lower OAFlux wind speeds are in the region of the South Equatorial Current where winds below with currents. The current effect is due primarily to the zonal component, while the effect of the meridional currents on meridional wind differences between OAFlux and buoy is less defined. It is found that the near-surface zonal currents derived from drifter measurements at 15-m depth [*Lumpkin and Garraffo*, 2005] can explain well the current effect on the mean differences between OAFlux and buoy winds in the SEC dominated regime. However, the climatology current estimates are too weak to account for the large discrepancies between OAFlux and buoy in the NECC-dominated regime (Figure 7).

[53] 3. The OAFlux wind synthesis encompasses three distinct periods: the QuikSCAT period (1999–2009) that has a near-complete global daily coverage and high-quality wind speed and direction retrievals, the pre-QuikSCAT period (1987–1999) that has only wind speed retrievals from SSMI series, and the post-QuikSCAT period (2009 onward) that features wind vector retrievals from ASCAT and wind speed retrievals from newer generation sensors. A comparison with buoy long-term daily time series suggested that the quality and accuracy of the OAFlux synthesis are consistent throughout the entire analysis period (Figures 11 and 12) and the degradation of the analysis for the pre-QuikSCAT period is small (Table 3).

[54] 4. Comparison of the performance of OAFlux with seven sensors (SSMI F13, SSMIS F16 and F17, AMSRE, WindSat, QuikSCAT, and ASCAT) was conducted using a total of 7660 collocations for the two-year period from 1 January 2008 to 31 December 2009. OAFlux has the smallest RMS differences (0.6 ms^{-1} in wind speed and 13 degrees in wind direction) and the best linear fit with buoys (Figures 13 and 14 and Table 4). Improvement of daily wind representation by the OAFlux synthesis is presented. It appears that the OAFlux framework of synergizing ASCAT, SSMIS and WindSat is able to compensate the loss of QuikSCAT after 2009.

[55] 5. ERA-interim surface winds provided the first guess to the OAFlux minimization and the background information for filling in data gaps caused by rain contamination or missing measurements. The study showed that OAFlux is a reasonable representation of the 12 input sensors and is not impacted by either biases or poor synoptic features in ERA-interim (Figures 15–17). Distinct decadal signals are seen in OAFlux, which differ considerably from the low-frequency behavior of ERA-interim winds (Figure 18).

[56] It should be noted that surface buoys are limited in the geographic coverage. Buoys are sparse, covering mostly the tropical oceans (Figures 2–4). They best characterize the tropical trade winds that have a wind speed in low and mid-range. They have irregular duration (Table 2), ranging from a few months at the field experiment sites in the extra-tropics to more than 10 years at some of the TAO/TRITON and PIRATA buoy sites. The time series of buoys are often fragmentary and the distance between buoys is so large that the buoys are insufficient for characterizing the either the temporal or spatial representation scales of a global analysis. Nonetheless, the 168,836 daily measurements from 126 buoys over the period of 1988–2010 are the best ground validation that one can have at present, and these buoy measurements have proven to be a useful benchmark for evaluating the accuracy and consistency of the OAFlux synthesis merged from 12 sensors over the satellite era. Characterizing temporal and spatial representation scales of OAFlux winds through cross-comparison with scatterometers and NWP models are being pursued in ongoing studies.

References

Alessi, C. A., S. J. Lentz, and R. C. Beardsley (1991), Shelf Mixed Layer Experiment (SMILE) program description and coastal and moored array data report, *Tech. Rep. 91–39*, Woods Hole Oceanogr. Inst., Woods Hole, Mass.

Atlas, R., R. N. Hoffman, J. Ardizzone, S. M. Leidner, J. C. Jusem, D. K. Smith, and D. Gombos (2011), A cross-calibrated, multiplatform ocean surface wind velocity product for meteorological and oceanographic applications, *Bull. Am. Meteorol. Soc.*, 92, 157–174, doi:10.1175/2010BAMS2946.1.

Attema, E. (1991), The Active Microwave Instrument onboard the ERS-1 satellite, *Proc. IEEE*, 79(6), 791–799, doi:10.1109/5.90158.

Bentamy, A., H.-L. Ayina, P. Queffeulou, and D. Croize-Fillon (2007), Improved near real time surface wind resolution over the Mediterranean Sea, *Ocean Sci.*, 3, 259–271, doi:10.5194/os-3-259-2007.

Bentamy, A., D. Croize-Fillon, and C. Perigaud (2008), Characterization of ASCAT measurements based on buoy and QuikSCAT wind vector observations, *Ocean Sci.*, 4, 265–274, doi:10.5194/os-4-265-2008.

Bentamy, A., S. A. Grodsky, J. A. Carton, D. Croizé-Fillon, and B. Chapron (2012), Matching ASCAT and QuikSCAT winds, *J. Geophys. Res.*, 117, C02011, doi:10.1029/2011JC007479.

Bourassa, M. A., D. M. Legler, J. J. O'Brien, and S. R. Smith (2003), SeaWinds validation with research vessels, *J. Geophys. Res.*, 108(C2), 3019, doi:10.1029/2001JC001028.

Bourassa, M. A., R. Romero, S. R. Smith, and J. J. O'Brien (2005), A new FSU winds climatology, *J. Clim.*, 18, 3686–3698, doi:10.1175/JCLI3487.1.

Bourlès, B., et al. (2008), The PIRATA Program: History, accomplishments, and future directions, *Bull. Am. Meteorol. Soc.*, 89, 1111–1125, doi:10.1175/2008BAMS2462.1.

Chelton, D. B., and M. H. Freilich, (2005), Scatterometer-based assessment of 10-m wind analyses from the operational ECMWF and NCEP numerical weather prediction models, *Mon. Weather Rev.*, 133, 409–429, doi:http://dx.doi.org/10.1175/MWR-2861.1.

Chelton, D. B., M. H. Freilich, J. M. Sienkiewitcz, and J. M. Von Ahn (2006), On the use of QuikSCAT scatterometer measurements of surface winds for marine weather prediction, *Mon. Weather Rev.*, 134, 2055–2071, doi:10.1175/MWR3179.1.

Chin, T. M., R. F. Milliff, and W. G. Large (1998), Basin-scale, high-wavenumber sea surface wind fields from a multiresolution analysis of scatterometer data, *J. Atmos. Oceanic Technol.*, 15, 741–763, doi:10.1175/1520-0426(1998)015<0741:BSHWSS>2.0.CO;2.

Colbo, K., and R. A. Weller (2009), The accuracy of the IMET sensor package in the subtropics, *J. Atmos. Oceanic Technol.*, 26(9), 1867–1890, doi:10.1175/2009JTECHO667.1.

Cronin, M. F., C. Meinig, C. L. Sabine, H. Ichikawa, and H. Tomita (2008), Surface mooring network in the Kuroshio Extension, *IEEE Syst. J.*, 2(3), 424–430.

Daley, R. (1991), *Atmospheric Data Analysis*, 457 pp., Cambridge Univ. Press, Cambridge, U. K.

Dee, D. P., et al. (2011), The ERA-Interim reanalysis: Configuration and performance of the data assimilation system, *Q. J. R. Meteorol. Soc.*, 137, 553–597, doi:10.1002/qj.828.

DeMoss, J. D., and K. Bowman (2007), Changes in TRMM rainfall due to the orbit boost estimated from buoy rain gauge data, *J. Atmos. Oceanic Technol.*, 24, 1598–1607.

Draper, D. W., and D. G. Long (2004), Evaluating the effect of rain on Sea-Winds scatterometer measurements, *J. Geophys. Res.*, 109, C02005, doi:10.1029/2002JC001741.

Ebuchi, N., H. C. Graber, and M. J. Caruso (2002), Evaluation of wind vectors observed by QuikSCAT/SeaWinds using ocean buoy data, *J. Atmos. Oceanic Technol.*, 19, 2049–2062, doi:10.1175/1520-0426(2002)019<2049:EOWVOB>2.0.CO;2.

Figa-Saldaña, J., J. J. W. Wilson, E. Attema, R. Gelsthorpe, M. R. Drinkwater, and A. Stoffelen (2002), The advanced scatterometer (ASCAT) on the meteorological operational (MetOp) platform: A follow on for European wind scatterometers, *Can. J. Remote Sens.*, 28(3), 404–412, doi:10.5589/m02-035.

Freilich, M. H. (1997), Validation of vector magnitude datasets: Effects of random component errors, *J. Atmos. Oceanic Technol.*, 14, 695–703, doi:10.1175/1520-0426(1997)014<0695:VOVMDE>2.0.CO;2.

Freilich, M. H., and R. S. Dunbar (1999), The accuracy of the NSCAT-1 vector winds: Comparisons with NDBC buoys, *J. Geophys. Res.*, 104, 11,231–11,246, doi:10.1029/1998JC900091.

Freilich, M. H., D. G. Long, and M. W. Spencer (1994), SeaWinds: A scanning scatterometer for ADEOS II—Science overview, paper presented at Geoscience and Remote Sensing Symposium 1994, IEEE, Pasadena, Calif.

Freitag, H. P., M. O'Haleck, G. C. Thomas, and M. J. McPhaden (2001), Calibration procedures and instrumental accuracies for ATLAS wind measurements, *NOAA Tech. Memo. OAR PMEL-119*, 20 pp., PMEL, NOAA, Seattle, Wash.

Gaiser, P. W., et al. (2004), The WindSat spaceborne polarimetric microwave radiometer: Sensor description and early orbit performance, *IEEE Trans. Geosci. Remote Sens.*, 42, 2347–2361, doi:10.1109/TGRS.2004.836867.

Gonzales, A. E., and D. G. Long (1999), An assessment of NSCAT ambiguity removal, *J. Geophys. Res.*, 104(C5), 11,449–11,457, doi:10.1029/98JC01943.

Häkkinen, S., and P. B. Rhines (2004), Decline of subpolar North Atlantic circulation during the 1990s, *Science*, 304, 555–559, doi:10.1126/science.1094917.

Hayes, S. P., M. J. McPhaden, and J. M. Wallace (1989), The influence of sea-surface temperature on surface wind in the eastern equatorial Pacific: Weekly to monthly variability, *J. Clim.*, 2(12), 1500–1506, doi:10.1175/1520-0442(1989)002<1500:TIOSST>2.0.CO;2.

Hilburn, K. A., F. J. Wentz, D. K. Smith, and P. D. Ashcroft (2006), Correcting active scatterometer data for the effects of rain using passive radiometer data, *J. Appl. Meteorol. Climatol.*, 45, 382–398, doi:10.1175/JAM2357.1.

Hoffman, R. N. (1984), SASS wind ambiguity removal by direct minimization. Part II: Use of smoothness and dynamical constraints, *Mon. Weather Rev.*, 112, 1829–1852, doi:10.1175/1520-0493(1984)112<1829:SWARBD>2.0.CO;2.

Hoffman, R. N., S. M. Leidner, J. M. Henderson, R. Atlas, J. V. Ardizzone, and S. C. Bloom (2003), A two-dimensional variational analysis method for NSCAT ambiguity removal: Methodology, sensitivity, and tuning, *J. Atmos. Oceanic Technol.*, 20, 585–605, doi:10.1175/1520-0426(2003)20<585:ATDVAM>2.0.CO;2.

Hollinger, J. P., J. L. Peirce, and G. A. Poe (1990), SSM/I instrument evaluation, *IEEE Trans. Geosci. Remote Sens.*, 28(5), 781–790, doi:10.1109/36.58964.

Jiang, C.-L., M. F. Cronin, K. A. Kelly, and L. Thompson (2005), Evaluation of a hybrid satellite and NWP based turbulent heat flux product using TAO buoys, *J. Geophys. Res.*, 110, C09007, doi:10.1029/2004JC002824.

Josey, S. A., E. C. Kent, and P. K. Taylor (2002), Wind stress forcing of the ocean in the SOC climatology: Comparisons with the NCEP–NCAR,

ECMWF, UWM/COADS, and Hellerman and Rosenstein datasets, *J. Phys. Oceanogr.*, *32*, 1993–2019, doi:10.1175/1520-0485(2002)032<1993:WSFOTO>2.0.CO;2.

Kako, S., A. Isobe, and M. Kubota (2011), High-resolution ASCAT wind vector data set gridded by applying an optimum interpolation method to the global ocean, *J. Geophys. Res.*, *116*, D23107, doi:10.1029/2010JD015484.

Kamphaus, R., M. Cronin, C. Sabine, S. Emerson, C. Meinig, and M. Robert (2008), New surface mooring at Station Papa monitors climate, *PICES Press*, *16*(2), 26–27.

Kawanishi, T., T. Sezai, Y. Ito, K. Imaoka, T. Takeshima, Y. Ishido, A. Shibata, M. Miura, H. Inahata, and R. Spencer (2003), The Advanced Microwave Scanning Radiometer for the Earth Observing System (AMSR-E), NASDA's contribution to the EOS for global energy and water cycle studies, *IEEE Trans. Geosci. Remote Sens.*, *41*(2), 184–194, doi:10.1109/TGRS.2002. 808331.

Kelly, K. A., S. Dickinson, M. J. McPhaden, and G. C. Johnson (2001), Ocean currents evident in satellite wind data, *Geophys. Res. Lett.*, *28*(12), 2469–2472, doi:10.1029/2000GL012610.

Kelly, K. A., S. Dickinson, and G. C. Johnson (2005), Comparisons of scatterometer and TAO winds reveal time-varying surface currents for the tropical Pacific Ocean, *J. Atmos. Oceanic Technol.*, *22*, 735–745, doi:10.1175/ JTECH1738.1.

Konda, M., H. Ichikawa, and H. Tomita (2009), Wind speed and latent heat flux retrieved by simultaneous observation of multiple geophysical parameters by AMSR-E, *J. Remote Sens. Soc. Jpn.*, *29*, 191–198.

Kundu, P. K. (1976), Ekman veering observed near the ocean bottom, *J. Phys. Oceanogr.*, *6*, 238–242.

Kunkee, D. B., G. A. Poe, D. J. Boucher, S. D. Swadley, Y. Hong, J. E. Wessel, and E. A. Uliana (2008), Design and evaluation of the First Special Sensor Microwave Imager/Sounder, *IEEE Trans. Geosci. Remote Sens.*, *46*(4), 863–883, doi:10.1109/TGRS.2008.917980.

Lau, K.-M., Y. P. Zhou, and H.-T. Wu (2008), Have tropical cyclones been feeding more extreme rainfall?, *J. Geophys. Res.*, *113*, D23113, doi:10.1029/ 2008JD009963.

Laursen, B., and N. Skou (2001), Wind direction over the ocean determined by an airborne, imaging, polarimetric radiometer system, *IEEE Trans. Geosci. Remote Sens.*, *39*(7), 1547–1555, doi:10.1109/36.934086.

Lumpkin, R., and Z. Garraffo (2005), Evaluating the decomposition of tropical Atlantic drifter observations, *J. Atmos. Oceanic Technol.*, *22*, 1403–1415, doi:10.1175/JTECH1793.1.

McPhaden, M. J., et al. (1998), The Tropical Ocean-Global Atmosphere observing system: A decade of progress, *J. Geophys. Res.*, *103*(C7), 14,169–14,240, doi:10.1029/97JC02906.

McPhaden, M. J., G. Meyers, K. Ando, Y. Masumoto, V. S. N. Murty, M. Ravichandran, F. Syamsudin, J. Vialard, L. Yu, and W. Yu (2009), RAMA: The Research Moored Array for African-Asian-Australian Monsoon Analysis and Prediction, *Bull. Am. Meteorol. Soc.*, *90*, 459–480, doi:10.1175/2008BAMS2608.1.

Mears, C. A., D. K. Smith, and F. J. Wentz (2001), Comparison of SSM/I and buoy-measured wind speeds from 1987–1997, *J. Geophys. Res.*, *106*(C6), 11,719–11,729, doi:10.1029/1999JC000097.

Meissner, T., and F. J. Wentz (2002), An updated analysis of the ocean surface wind direction signal in passive microwave brightness temperatures, *IEEE Trans. Geosci. Remote Sens.*, *40*(6), 1230–1240, doi:10.1109/ TGRS.2002.800231.

Milliff, R. F., and J. Morzel (2001), The global distribution of the time-average wind stress curl from NSCAT, *J. Atmos. Sci.*, *58*, 109–131, doi:10.1175/1520-0469(2001)058<0109:TGDOTT>2.0.CO;2.

Milliff, R. F., J. Morzel, D. B. Chelton, and M. H. Freilich (2004), Wind stress curl and wind stress divergence biases from rain effects on QSCAT surface wind retrievals, *J. Atmos. Oceanic Technol.*, *21*, 1216–1231, doi:10.1175/1520-0426(2004)021<1216:WSCAWS>2.0.CO;2.

Moyer, K. A., and R. A. Weller (1997), Observations of surface forcing from the Subduction experiment: A comparison with global model products and climatological data sets, *J. Clim.*, *10*, 2725–2742, doi:10.1175/ 1520-0442(1997)010<2725:OOSFFT>2.0.CO;2.

Naderi, F., M. H. Freilich, and D. G. Long (1991), Spaceborne radar measurement of wind velocity over the ocean—An overview of the NSCAT system, *Proc. IEEE*, *79*(6), 850–866, doi:10.1109/5.90163.

Payne, R. E., et al. (2002), A comparison of buoy meteorological systems, *Tech. Rep. WHOI-2002–10*, 67 pp., Woods Hole Oceanogr. Inst., Woods Hole, Mass.

Portabella, M., and A. Stoffelen (2001), Rain detection and quality control of SeaWinds, *J. Atmos. Oceanic Technol.*, *18*(7), 1171–1183, doi:10.1175/ 1520-0426(2001)018<1171:RDAQCO>2.0.CO;2.

Portabella, M., and A. C. M. Stoffelen (2009), On scatterometer ocean stress, *J. Atmos. Oceanic Technol.*, *26*(2), 368–382, doi:10.1175/2008JTECHO578.1.

Quilfen, Y., C. Prigent, B. Chapron, A. A. Mouche, and N. Houti (2007), The potential of QuikSCAT and WindSat observations for the estimation of sea surface wind vector under severe weather conditions, *J. Geophys. Res.*, *112*, C09023, doi:10.1029/2007JC004163.

Risien, C. M., and D. B. Chelton (2008), A global climatology of surface wind and wind stress fields from eight years of QuikSCAT scatterometer data, *J. Phys. Oceanogr.*, *38*, 2379–2413, doi:10.1175/2008JPO3881.1.

Stiles, B. W., and S. H. Yueh (2002), Impact of rain on spaceborne Ku-band wind scatterometer data, *IEEE Trans. Geosci. Remote Sens.*, *40*, 1973–1983, doi:10.1109/TGRS.2002.803846.

Stoffelen, A., and A. Verhoef (2011), OCEANSAT-2 scatterometer winds and sea ice, paper presented at 2011 EUMETSAT Meteorological Satellite Conference, EUMETSAT, Oslo.

Tang, W., and W. T. Liu (1996), Equivalent neutral wind, *JPL Publ.*, *96-17*, 16 pp.

Tournadre, J., and Y. Quilfen (2003), Impact of rain cell on scatterometer data: 1. Theory and modeling, *J. Geophys. Res.*, *108*(C7), 3225, doi:10.1029/ 2002JC001428.

Verhoef, A., and A. Stoffelen (2012a), OceanSat-2 wind product user manual version 1.1, *SAF/OSI/CDOP/KNMI/TEC/MA/140*, 27 pp., EUMETSAT, KNMI, De Bilt, Netherlands. [Available at http://www. knmi.nl/publications/fulltexts/ss3_pm_oscat_1.1.pdf.]

Verhoef, A., and A. Stoffelen (2012b), ASCAT wind product user manual version 1.12, *SAF/OSI/CDOP/KNMI/TEC/MA/126*, 27 pp., EUMETSAT, KNMI, De Bilt, Netherlands. [Available at http://www.knmi.nl/publications/fulltexts/ss3_pm_ascat_1.12.pdf.]

Verspeek, J., A. Verhoef, and A. Stoffelen (2010), ASCAT NWP ocean calibration, report, 36 pp., KNMI, De Bilt, Netherlands. [Available at http:// www.knmi.nl/publications/fulltexts/ascat_nwp_ocean_calibration_1.5_copy1. pdf.]

Vogelzang, J., A. Stoffelen, A. Verhoef, and J. Figa-Saldaña (2011), On the quality of high-resolution scatterometer winds, *J. Geophys. Res.*, *116*, C10033, doi:10.1029/2010JC006640.

Wallcraft, A. J., A. B. Kara, C. N. Barron, E. J. Metzger, R. L. Pauley, and M. A. Bourassa (2009), Comparisons of monthly mean 10 m wind speeds from satellites and NWP products over the global ocean, *J. Geophys. Res.*, *114*, D16109, doi:10.1029/2008JD011696.

Weissman, D. E., M. A. Bourassa, and J. Tongue (2002), Effects of rain rate and wind magnitude on SeaWinds scatterometer wind speed errors, *J. Atmos. Oceanic Technol.*, *19*, 738–746, doi:10.1175/1520-0426(2002) 019<0738:EORRAW>2.0.CO;2.

Weller, R. A., and S. P. Anderson (1996), Surface meteorology and air-sea fluxes in the western equatorial Pacific warm pool during the TOGA Coupled Ocean-Atmosphere Response Experiment, *J. Clim.*, *9*(8), 1959–1990, doi:10.1175/1520-0442(1996)009<1959:SMAASF>2.0.CO;2.

Wentz, F. J. (1997), A well-calibrated ocean algorithm for SSM/I, *J. Geophys. Res.*, *102*(C4), 8703–8718, doi:10.1029/96JC01751.

Wentz, F. J., T. Meissner, and D. K. Smith (2005), Assessment of the WindSat retrievals produced by NRL, *RSS Tech. Rep. 010605*, 32 pp., Remote Sens. Syst., Santa Rosa, Calif.

Young, I. R., S. Zieger, and A. V. Babanin (2011), Global trends in wind speed and wave height, *Science*, *332*, 451–455, doi:10.1126/science. 1197219.

Yu, L. (2007), Global variations in oceanic evaporation (1958–2005): The role of the changing wind speed, *J. Clim.*, *20*, 5376–5390.

Yu, L. (2009), Sea surface exchanges of momentum, heat, and freshwater determined by satellite remote sensing, in *Encyclopedia of Ocean Sciences*, 2nd ed., edited by J. Steele, S. Thorpe, and K. Turekian, pp. 202–211, Academic, London, doi:10.1016/B978-012374473-9.00800-6.

Yu, L., and R. A. Weller (2007), Objectively Analyzed air-sea heat Fluxes (OAFlux) for the global ocean, *Bull. Am. Meteorol. Soc.*, *88*(4), 527–539, doi:10.1175/BAMS-88-4-527.

Yu, L., X. Jin, and R. Weller (2008), Multidecade global flux datasets from the Objectively Analyzed Air-sea Fluxes (OAFlux) Project: Latent and sensible heat fluxes, ocean evaporation, and related surface meteorological variables, *OAFlux Project Tech. Rep. OA-2008–01*, 64 pp., Woods Hole Oceanogr. Inst., Woods Hole, Mass.

Yueh, S. H., and W. J. Wilson (1999), Validation of wind radiometer technique using aircraft radiometer and radar measurements for high ocean winds, *JPL Rep. D-17815*, Jet Propul. Lab., Pasadena, Calif.

Yueh, S. H., W. J. Wilson, F. K. Li, S. Y. Nghiem, and W. B. Ricketts (1995), Polarimetric measurements of the sea surface brightness temperature using an aircraft K-band radiometer, *IEEE Trans. Geosci. Remote Sens.*, *33*(1), 85–92, doi:10.1109/36.368219.

Zhang, H.-M., J. J. Bates, and R. W. Reynolds (2006), Assessment of composite global sampling: Sea surface wind speed, *Geophys. Res. Lett.*, *33*, L17714, doi:10.1029/2006GL027086.